Analytical and Semi-analytical Solutions for Describing Tunneling-induced Transverse and Longitudinal Settlement Troughs

Pin ZHANG[1], Zhen-Yu YIN[1], Ren-Peng CHEN M. ASCE[2]*

1. Department of Civil and Environmental Engineering, The Hong Kong Polytechnic University, Hung Hom, Kowloon, Hong Kong, China;

2. College of Civil Engineering, Hunan University, Changsha 410082, China

Corresponding author: Ren-Peng CHEN; Email: chenrp@hnu.edu.cn

Abstract: It is still an open problem to develop a solution to predict ground deformation induced by shallow tunnels construction in dry soils. This study proposes a closed-form elastic analytical solution and a plastic analytical solution for calculating longitudinal settlement trough. Meanwhile a semi-analytical solution is further developed for better fitting tunneling-induced ground deformation, in which the metaheuristics optimization algorithm particle swarm optimization (PSO) is employed to identify the empirical parameters of the proposed semi-analytical solution. A uniform formulation with the combination of analytical and semi-analytical solutions that accounts for tunnel uniform convergence and ovalization deformation modes is ultimately proposed. A 3-dimension numerical modelling and centrifuge test results are used to validate the prediction capability of the proposed solutions in predicting longitudinal and transverse settlement troughs, respectively. The results indicate proposed semi-analytical solution can overcome the deficiency of analytical solutions, and the predicted results show great agreement with actual tunneling-induced transverse and longitudinal settlement troughs. A simple linear relationship is discovered between coefficients of the proposed semi-analytical solution identified by PSO and their influential factors, which assigns physical meaning to these empirical coefficients and also provides a straightforward method to

estimate coefficients in an effective way.

Keywords: Tunnel; Settlement; Analytical solution; Optimization; Numerical modelling; Centrifuge modelling

Introduction

Shallow metro tunnels are rapidly constructing in large cities of China for mitigating increasingly traffic congestion arising from urbanization (Lü et al. 2017; Zhang et al. 2020; Zhang and Huang 2014). Ground deformation inevitably occurs during the tunneling process due to the stress relief, over-excavation and tail void, which occasionally poses a threat to surrounding structures and infrastructures, especially in the densely populated area (Chen et al. 2018; Zheng et al. 2017; Zheng et al. 2018). Numerous researchers have thus been preoccupied with the development of approaches, i.e. empirical methods (Peck 1969; Vorster et al. 2005), analytical and semi-analytical solutions (Bobet 2001; Loganathan and Poulos 1998; Sagaseta 1987; Verruijt 1997; Verruijt and Booker 1996; Yang et al. 2004), numerical and physical modelling (Fang et al. 2019; Hu et al. 2019; Ng et al. 2013), and advanced machine learning-based models (Chen et al. 2019; Chen et al. 2019; Zhang 2019; Zhang et al. 2019) to predict tunneling-induced settlement for avoiding risks.

In spite of the complex soil-tunnel interaction taking place around the tunnel, numerous field and laboratory experiments indicate the soil deformation pattern at some distance from tunnel centerline ~~are~~is relatively smooth. This motivates the development of a general approach, in which the tunneling process is not reproduced by themselves, but represented by their overall effects on the ground deformation, i.e. ground volume loss (González and Sagaseta 2001). Hence, most empirical, analytical, semi-analytical, numerical and physical modelling methods were developed based on this conception. Tunneling-induced ground settlement has been extensively described by empirical formulations in engineering practice due to theirs simplicity and well description of settlement trough shape (Peck 1969; Suwansawat and Einstein 2007; Wang et al. 2018). Nevertheless, empirical methods such as Gaussian curve are merely applicable for limited cases, e.g. tunneling-induced settlement in normally consolidated clays, and tend to be misleading in the granular medium and overconsolidated clays (New and O'Reilly 1991). Therefore, accurate and user-friendly closed-form analytical and semi-analytical solutions that can account for soil-tunnel interaction mechanism instead of such phenomenological methods deserve to be developed.

Regarding tunneling-induced transverse settlement trough, Sagaseta (1987) first utilized point sink and virtual image methods to calculate uniform ground volume loss induced displacement of isotropic and homogeneous incompressible soils in an elastic half-space. Verruijt and Booker (1996) further extended Sagaseta (1987)'s solution to account for ground compressibility and the tunnel ovalization deformation mode. González and Sagaseta (2001) modified Verruijt and Booker (1996)'s solution to account for plastic volumetric strain of incompressible soils (v = 0.5). Such three analytical solutions provide a basis for the future development of closed-form analytical and semi-analytical solutions (Franza and Marshall 2015; Franza and Marshall 2015; Fu et al. 2016; Park 2004; Yuan et al. 2018). Relatively few closed-form analytical solutions have been made to predict tunneling-induced longitudinal settlement trough. Based on 3-dimension deformation field induced by the nucleus of elastic strain (Sen 1951), Sagaseta (1987) and Pinto and Whittle (2014) have proposed closed-form analytical solutions to calculate longitudinal settlement trough induced by the uniform ground volume loss, but this solution exists some deficiencies, e.g. cannot account for complicated ground deformation mode and 50% of the total settlement always completes when the tunnel face reaches the monitoring section. Therefore, current published analytical and semi-analytical solutions for transverse settlement trough are miscellaneous and some of them are not practical for engineering practice, meanwhile the development of solutions for longitudinal settlement trough are not sufficient enough.

This study aims to develop novel closed-form analytical and semi-analytical solutions to predict transverse and longitudinal settlement troughs induced by shallow tunnel construction. The first part of this study presents a very comprehensive literature review regarding ~~experimental~~ empirical, analytical and semi-analytical approaches for calculating ground deformation. Thereafter, an elastic analytical solution and a plastic analytical solution for incompressible medium with the integration of tunnel ovalization deformation mode are proposed. Due to the limitation of analytical solutions, a semi-analytical solution modified by corrective terms is further developed for better fitting transverse and longitudinal settlement troughs. Herein, a metaheuristics optimization algorithm particle swarm optimization (PSO) is employed to identify the coefficients of corrective terms and investigate the relationships between such coefficients and their influential factors. A uniform formulation is ultimately proposed with the integration of currently prevailing and proposed analytical and semi-analytical solutions for comparing the applicability of various solutions. Consequently, a 3-dimension numerical model is established to compare and validate the performance of various solutions in predicting longitudinal settlement trough, and centrifuge test results from a published research is utilized to compare the prediction capability in transverse settlement trough.

Literature review

Transversal settlement trough

Empirical methods

In the greenfield condition, Peck (1969) has pointed out that the tunneling-induced transverse settlement trough is well described using a standard Gaussian curve:

$$\mu_z = \mu_{z,\max} \exp\left(-\frac{x^2}{2i^2}\right) \quad (1)$$

where μ_z = vertical settlement; $\mu_{z,\max}$ = maximum settlement; x = horizontal distance from the tunnel centerline; i = horizontal distance from the tunnel centerline to the inflection point of settlement curve.

By integrating Eq. [1], the volume of ground surface settlement trough V_s can be obtained by:

$$V_s = \sqrt{2\pi} i \mu_{z,\max} \tag{2}$$

The ground volume loss V_t refers to the volume loss in the vicinity of the tunnel. V_t is generally not equal to V_s because of soil dilation or contraction during tunneling process, and $V_t = V_s$ merely occurs if the soils are incompressible (constant volume). The volume of ground surface settlement V_s and ground volume loss V_t is expressed as a percentage of the area of tunnel cross-section:

$$V_s = V_{l,s} * \pi R^2 \tag{3}$$

$$V_t = V_{l,t} * \pi R^2 \tag{4}$$

where R = radius of tunnel; $V_{l,s}$ and $V_{l,t}$ hereafter donate the volume loss of ground surface and ground volume loss around tunnel. Integration of Eqs. [1]–[3] gives:

$$\mu_z = \frac{V_{l,s} \pi R^2}{\sqrt{2\pi} i} \exp\left(-\frac{x^2}{2i^2}\right) \tag{5}$$

Therefore, numerous empirical methods have been developed to calculate i at various depth (Chakeri et al. 2014; Mair et al. 1993), whereas $V_{l,s}$ is generally summarized based on different soil types, tunnel construction methods, etc (Dindarloo and Siami-Irdemoosa 2015). Because of the failure to accurately describe the tunneling-induced transverse settlement trough in many cases such as in drained soils, some substituted formulations for describing transverse settlement trough were proposed by Celestino et al. (2000), Jacobsz et al. (2004) and Vorster et al. (2005), respectively, as shown in following:

$$\mu_z = \frac{\mu_{z,\max}}{1 + \left(\frac{|x|}{a}\right)^b} \tag{6}$$

$$\mu_z = \mu_{z,\max} \exp\left[-\frac{1}{3}\left(\frac{|x|}{i}\right)^{1.5}\right] \tag{7}$$

$$\left.\begin{aligned} \mu_z &= \mu_{z,\max} \frac{n}{(n-1)+\exp\left[\alpha\left(\frac{x}{i}\right)^2\right]} \\ n &= \frac{2\alpha-1}{2\alpha+1}e^m+1 \end{aligned}\right\} \tag{8}$$

where *a* = length dimension parameter; *b* = dimensionless parameter; *n* = shape parameter for controlling the width of the settlement trough; *m* = parameter for ensuring that horizontal distance from the tunnel centerline to the inflection point of settlement curve remains constant with the change in the *m*.

Herein, Eq. [6] uses a yield-density curve for describing settlement trough, and Eq. [7] is a slightly different version of the Gaussian curve. Eq. [8] is a modified Gaussian curve with an additional parameter~~s~~ *m*. For the case of *n* = 1, the Vorster et al. (2005)'s modified Gaussian curve is the same as a standard Gaussian curve. It can be seen from Fig. 1 that the shape of settlement trough narrows with the increase in *n*, meanwhile the settlement trough width *i* maintains constant. Herein, the settlement has been normalized for clearly comparing the effect of studied parameters on the settlement trough shape. Therefore, this method is more appropriate to describe tunneling-induced transverse settlement trough, because it can flexibly adjust the shape of transverse settlement trough with a constant *i*. Nevertheless, the parameter *m* lacks a physical meaning. Marshall et al. (2012) suggested to characterize the shape of settlement trough using two points of any empirical curves (Eqs. [1], [6]–[8]), that is, (x^*, 0.606$\mu_{z,\max}$) and (x^{**}, 0.303$\mu_{z,\max}$). The corresponding values of trough width parameters are represented by K^* and K^{**}. Thereafter a correlation between (m, i, $\mu_{z,\max}$) and (K^*, K^{**}, $V_{l,s}$) can be obtained by:

$$\left.\begin{aligned}
&m \approx 10^{-7}\exp\left[-17.5\left(\frac{K^{*}}{K^{**}}\right)^{2}+35.5\left(\frac{K^{*}}{K^{**}}\right)\right]-0.11\\
&i=\sqrt{\frac{m}{\mathrm{In}\left[n\sqrt{e}-\left(n-1\right)\right]}}\times K^{*}\left(h-z\right)\\
&\mu_{z,\max}\approx\frac{\sqrt{2\pi}}{\exp\left(1.7+0.52m-1.47\sqrt{m}\right)}\times\frac{V_{l,s}\,\pi R^{2}}{100i\sqrt{2\pi}}
\end{aligned}\right\} \tag{9}$$

where h = depth of tunnel axis. The detailed deduction can refer to Franza and Marshall (2019). This method assigns the physical meaning of each parameters of Eq. [8], but it is certainly less user-friendly than the conventional formulations.

Analytical solutions

Closed-form analytical solutions for describing tunneling-induced settlement trough depend on simplified assumptions regarding the constitutive behavior of soil, meanwhile fulfill the principles of continuum mechanics and boundary conditions. The most fundamental assumptions of current analytical methods involve the deformation mode of tunnel cavity and soil volumetric behavior. The deformation of tunnel cavity is now acceptably categorized into three modes: (*i*) uniform convergence, μ_{ε}; (*ii*) ovalization, $\mu_{\delta,\max}$; (*iii*) vertical translation, $\Delta\mu_z$ (see Fig. 2) (González and Sagaseta 2001). Both elastic and plastic volumetric behavior of soils are taken into account (González and Sagaseta 2001; Sagaseta 1987; Verruijt and Booker 1996).

The analytical solutions for tunneling-induced settlement can be regarded as a displacement–displacement problem, in which displacement is imposed around the tunnel and only the resulting displacement field is obtained. Sagaseta (1987) first utilized point sink method to calculate uniform ground volume loss induced displacement of isotropic and homogeneous incompressible soils in an elastic infinite half-space, and a virtual image technique was employed to satisfy the boundary condition of the top surface (see Fig. 3). The horizontal and vertical deformations of ground surface under 2-dimension plain strain condition are obtained:

$$\mu_{x,z=0} = -2\varepsilon R^2 \frac{x}{x^2+h^2} \tag{10a}$$

$$\mu_{z,z=0} = 2\varepsilon R^2 \frac{h}{x^2+h^2} \tag{10b}$$

where ε = normalized convergence deformation, μ_ε/R.

Verruijt and Booker (1996) further extended the method proposed by Sagaseta (1987) to account for ground compressibility and the tunnel ovalization deformation mode, and both uniform convergence and tunnel ovalization can generate vertical translation deformation (Pinto and Whittle 2014). The corresponding ground deformation under 2-dimension plain strain condition can be expressed by:

$$\begin{aligned}\mu_x = {} & -\varepsilon R^2\left(\frac{x}{r_1^2}+\frac{x}{r_2^2}\right)+\delta R^2\left[\frac{x\left(x^2-kz_1^2\right)}{r_1^4}+\frac{x\left(x^2-kz_2^2\right)}{r_2^4}\right] \\ & -2\varepsilon R^2\left[\frac{x\left(1-2\nu\right)}{r_2^2}-\frac{2xzz_2}{r_2^4}\right]-4\delta R^2 h\left[\frac{\left(1-2\nu\right)z_2 x}{\left(2-2\nu\right)r_2^4}+\frac{xz(x^2-3z_2^2)}{\left(2-2\nu\right)r_2^6}\right]\end{aligned} \tag{11a}$$

$$\begin{aligned}\mu_z = {} & -\varepsilon R^2\left(\frac{z_1}{r_1^2}+\frac{z_2}{r_2^2}\right)+\delta R^2\left[\frac{z_1\left(kx^2-z_1^2\right)}{r_1^4}+\frac{z_2\left(kx^2-z_2^2\right)}{r_2^4}\right] \\ & +2\varepsilon R^2\left[\frac{2\left(1-\nu\right)z_2}{r_2^2}-\frac{z\left(x^2-z_2^2\right)}{r_2^4}\right]-2\delta R^2 h\left[\frac{x^2-z_2^2}{r_2^4}+\frac{2zz_2\left(3x^2-z_2^2\right)}{2\left(1-\nu\right)r_2^6}\right]\end{aligned} \tag{11b}$$

The horizontal and vertical settlement at the ground surface z = 0 is:

$$\mu_{x,z=0} = -2\varepsilon R^2 \frac{x\left(2-2\nu\right)}{x^2+h^2}+2\delta R^2\left[\frac{x\left(x^2-kh^2\right)}{\left(x^2+h^2\right)^2}-\frac{2h^2x\left(1-2\nu\right)}{\left(2-2\nu\right)\left(x^2+h^2\right)^2}\right] \tag{12a}$$

$$\mu_{z,z=0} = 2\varepsilon R^2 \frac{2\left(1-\nu\right)h}{x^2+h^2}-2\delta R^2 h\frac{x^2-h^2}{\left(x^2+h^2\right)^2} \tag{12b}$$

where ν = Poisson's ratio, which is used to account for ground compressibility; $k = \nu/(1-\nu)$; δ = normalized tunnel ovalization deformation, $\mu_{\delta,max}/R$. $z_1 = z - h$; $z_2 = z + h$; $r_1^2 = x^2 + z_1^2$; $r_2^2 = x^2 + z_2^2$. The first term donates the horizontal and vertical settlement caused by tunnel uniform convergence, and the second term is caused by tunnel ovalization. For the case of v = 0.5, which donates soils are incompressible, the first term is the same as the solutions proposed by Sagaseta (1987). The relative distortion of tunnel, $\rho = \delta/\varepsilon$, could be an alternative way for describing the tunnel ovalization. It can be seen from Fig. 4(a) that the tunnel overlization obviously decreases the width of settlement trough, and the width of settlement trough decreases with the increase in ρ. It can be observed that the increase in the Poisson's ratio can slightly decreases the width of settlement trough, but this effect is not discernable, compared with the tunnel ovalization. Therefore, the predicted width of settlement trough using Verruijt and Booker (1996)'s method is narrower than that predicted by Sagaseta (1987)'s solution.

González and Sagaseta (2001) modified Verruijt and Booker (1996)'s solution to account for the plastic volumetric strain of incompressible soils (v = 0.5). The displacements in the plastic zone for non-elastic medium attenuate with a power of the distance, $O(1/r^{\alpha})$ is the basic assumption of this solution. The corresponding ground deformation under 2-dimension plain strain condition can be expressed by:

$$\begin{aligned}\frac{\mu_x}{2\varepsilon R\left(\dfrac{R}{h}\right)^{2\alpha-1}} = &-\frac{x}{2r_1^{2\alpha}h^{1-2\alpha}}\left(1-\rho\frac{x^2-z_1^2}{r_1^2}\right)-\frac{x}{2r_2^{2\alpha}h^{1-2\alpha}}\left(1-\rho\frac{x^2-z_2^2}{r_2^2}\right)\\ &+\frac{4xz}{2r_2^{2\alpha}h^{2-2\alpha}}\left(h\frac{z_2}{r_2^2}-\rho h^2\frac{x^2-3z_2^2}{r_2^4}\right)\end{aligned} \tag{13a}$$

$$\begin{aligned}\frac{\mu_z}{2\varepsilon R\left(\dfrac{R}{h}\right)^{2\alpha-1}} = &-\frac{z_1}{2r_1^{2\alpha}h^{1-2\alpha}}\left(1-\rho\frac{x^2-z_1^2}{r_1^2}\right)+\frac{z_2}{2r_2^{2\alpha}h^{1-2\alpha}}\left(1+\rho\frac{x^2-z_2^2}{r_2^2}\right)\\ &-\frac{1}{2r_2^{2\alpha}h^{-2\alpha}}\left[2\left(\frac{z}{h}+\rho\right)\frac{x^2-z_2^2}{r_2^2}+4\rho z z_2\frac{3x^2-z_2^2}{r_2^4}\right]\end{aligned} \tag{13b}$$

The horizontal and vertical settlement at the ground surface z = 0 is:

$$\mu_{x,z=0} = -2\varepsilon R\left(\frac{R}{h}\right)^{2\alpha-1}\frac{x}{\left(x^2+h^2\right)^{\alpha}h^{1-2\alpha}}\left(1-\rho\frac{x^2-h^2}{x^2+h^2}\right) \tag{14a}$$

$$\mu_{z,z=0} = 2\varepsilon R\left(\frac{R}{h}\right)^{2\alpha-1}\frac{1}{\left(x^2+h^2\right)^{\alpha}h^{-2\alpha}}\left(1-\rho\frac{x^2-h^2}{x^2+h^2}\right) \tag{14b}$$

where α = average value of ground compressibility parameter, generally in the range of 1.0–2.0. González and Sagaseta (2001)'s solutions for the case of α = 1 is the same as the Verruijt and Booker (1996)'s solutions. It can be seen from Fig. 4(b) that the increase in α can decrease the width of settlement trough, which complies with the results observed in engineering practice. Overall, regarding analytical solutions for calculating transverse settlement trough, the tunnel deformation mode is the primary parameter affecting the shape of settlement trough, compared with soils properties. Without consideration of the tunnel ovalization, the predicted settlement trough may be much wider than measured results.

Semi-analytical solutions

Loganathan and Poulos (1998) pointed out that ground volume loss was affected by tunneling methods, tunnel configuration, soil types, etc, and a gap parameter g was able to be employed to represent ground volume loss for comprehensively accounting for these influential factors. Meanwhile only a non-uniform convergence deformation mode around tunnel was considered, and its distribution was empirically defined as:

$$\varepsilon_{x,z} = \frac{4gR+g^2}{4R^2}\exp\left\{-\left[\frac{1.38x^2}{\left(h+R\right)^2}+\frac{0.69z^2}{h^2}\right]\right\} \tag{15}$$

By combination with the Verruijt and Booker (1996)'s analytical solution, Loganathan and Poulos (1998) proposed a semi-analytical solution, in which they merely considered a non-uniform convergence deformation mode. Therefore, this semi-analytical solution was easily derived with the integration of Eqs. [10] and [15]. The horizontal and vertical settlement at the ground surface z = 0 are:

$$\mu_{x,z=0} = -R^2 x\left[\frac{1}{x^2+h^2}+\frac{3-4v}{x^2+h^2}\right]\frac{4gR+g^2}{4R^2}\exp\left[-\frac{1.38x^2}{\left(h+R\right)^2}\right] \tag{16a}$$

$$\mu_{z,z=0} = 4(1-v)R^2 \frac{h}{h^2+x^2}\frac{4gR+g^2}{4R^2}\exp\left[-\frac{1.38x^2}{(h+R)^2}\right] \tag{16b}$$

Another semi-analytical solution based on Verruijt and Booker (1996)'s analytical solution was proposed by Franza and Marshall (2019). This semi-analytical solution involved two basic assumptions: (i) soils are incompressible (v = 0.5); (ii) ρ = 1 ($\varepsilon = \delta$) deprived from the centrifuge results in which the horizontal movements measured at the tunnel springline are negligible across the range of volume losses considered ($V_{l,t}$ = 0−5%). Meanwhile, two corrective terms: ξ_x and ξ_z are applied in the horizontal and vertical deformation, respectively, as shown following:

$$\mu_x = -2\varepsilon R^2 \xi_x \left\{ \frac{x}{2r_1^2}\left[1-\frac{(x^2-z_1^2)}{r_1^2}\right] + \frac{x}{2r_2^2}\left[1-\frac{(x^2-z_2^2)}{r_2^2}\right] - \frac{4xz}{2r_2^4}\left[z_2 - \frac{h(x^2-3z_2^2)}{r_2^2}\right] \right\} \tag{17a}$$

$$\mu_z = -2\varepsilon R^2 \xi_z \left\{ \frac{z_1}{2r_1^2}\left[1-\frac{(x^2-z_1^2)}{r_1^2}\right] - \frac{z_2}{2r_2^2}\left[1+\frac{(x^2-z_2^2)}{r_2^2}\right] + \frac{1}{2r_2^4}\left[2(z+h)(x^2-z_2^2)+4hzz_2\frac{3x^2-z_2^2}{r_2^2}\right] \right\} \tag{17b}$$

Empirical correlations between coefficients ξ_x, ξ_z and ground volume loss, cover-to-diameter ratio, soil relative density were established by Franza and Marshall (2019) based on the centrifuge experimental results.

Longitudinal settlement trough

Empirical methods

A cumulative probability function was proposed by New and O'Reilly (1991) for describing tunneling-induced longitudinal settlement trough. The vertical settlement of ground surface along the tunnel advance direction can be determined by:

$$\mu_{z,z=0} = \mu_{z,\max}\exp\left(-\frac{x^2}{2i^2}\right)\left[G\left(\frac{y-y_i}{i}\right)-G\left(\frac{y-y_f}{i}\right)\right] \tag{18}$$

where y_i = initial position of tunnel; y_f = position of current tunnel face; The value of $G(x)$ can be determined from a standard probability table.

Analytical solutions

The integration of point sink and virtual image methods can also be employed to calculate 3-dimension ground deformation for a spherical cavity point embedded at depth h in an elastic half-space. For the case of ground volume loss uniformly distributed along the tunnel axis, $V_{l,t} = 2\varepsilon\pi R^2$ (see Fig. 5(a)), the ground surface settlement for incompressible soils along the tunnel axis can be obtained by Sagaseta (1987):

$$\mu_{z,z=0} = \varepsilon R^2 \frac{h}{x^2+h^2}\left[1-\frac{y}{\left(x^2+y^2+h^2\right)^2}\right] \tag{19}$$

The 3-dimension ground deformation contour for $h/R = 3$ calculated by Eq. [19] can be seen in Fig. 5(b). The corresponding longitudinal settlement trough at the tunnel axis, $x = 0$, is presented in Fig. 5(c). It can be seen from Eq. [19] that settlement increases linearly with the tunnel uniform convergence. Regarding the tunnel depth, it can be observed in Fig. 5(c) that the settlement is limited to a zone around the tunnel face with the y/h in the range of –4 to 4, and the evolution of settlement is similar to the tunnel buried at various depth. For any case, 50% of the total settlement completes when the tunnel face reaches monitoring section.

Proposed semi-analytical solutions

Analytical solution for longitudinal ground deformation

The published research works primarily focused on developing solutions for describing transverse settlement trough, whereas relatively few solutions are proposed for calculating longitudinal settlement. In reality, 3-dimension deformation field induced by the nucleus of elastic strain at (0, 0, h) in the isotropic semi-infinite elastic space has earlier been derived by Sen (1951).

$$\mu_x = \frac{V_L}{4\pi} x\left[\frac{1}{R_1^3}+\frac{(3-4v)}{R_2^3}-\frac{6z(z+h)}{R_2^5}\right] \tag{20a}$$

$$\mu_y = \frac{V_L}{4\pi} y \left[\frac{1}{R_1^3} + \frac{(3-4v)}{R_2^3} - \frac{6z(z+h)}{R_2^5} \right] \tag{20b}$$

$$\mu_z = \frac{V_L}{4\pi} \left[\frac{z-h}{R_1^3} + \frac{4v(z+h)-(z+3h)}{R_2^3} - \frac{6z(z+h)^2}{R_2^5} \right] \tag{20c}$$

where, V_L = volumetric loss at (0, 0, h); $R_1 = \sqrt{x^2 + y^2 + (z-h)^2}$; $R_2 = \sqrt{x^2 + y^2 + (z+h)^2}$. Based on Sen (1951)'s solution, tunneling-induced 3-dimension deformation field resulting from the prescribed distributions of ground volume loss can be obtained. Sagaseta (1987) and Pinto and Whittle (2014) have thus proposed Eq. [19] for calculating 3-dimension deformation field induced by the uniform ground volume loss, i.e., the ground volume loss is uniformly distributed along the tunnel axis. This study further develops this solution based on Sen (1951)'s solution with the integration of tunnel ovalization deformation mode for better describing tunneling-induced longitudinal settlement trough. The proposed elastic analytical solution and plastic analytical solution for incompressible medium to calculate longitudinal settlement trough at the ground surface are shown in Appendix I.

Corrective term

Analytical solutions are limited to simple soil deformation modes, i.e. elastic and plastic (with a fixed attenuation rule) deformation. They tend to mislead certain settlement characteristics, e.g. 50% of the total settlement always completes when the tunnel face reaches the monitoring section, as shown in Fig. 5(c). Therefore, semi-analytical solution combined with corrective terms is proposed for improving its accuracy and applicability. The two corrective terms ξ_x and ξ_z (see Eq. [21]), which are motivated by Franza and Marshall (2019), are proposed for refining the vertical and horizontal ground deformation. Franza and Marshall (2019)'s corrective terms were able to refine ground deformation in a 2-dimension plain. Such two corrective terms are further extended by adding an additional coefficient in the y direction to describe tunneling-induced settlement in a 3-dimension space with a simpler formulation.

$$\xi_x^p = c_{A,x}\exp\left\{-\left[c_{1,x}\left(\frac{x}{h}\right)^2 + c_{2,x}\left(\frac{y}{h}\right) + c_{3,x}\left(\frac{z}{h}\right)^2\right]\right\} + c_{B,x}\exp\left\{-\left[c_{4,x}\left(\frac{x}{h}\right)^2 + c_{5,x}\left(\frac{y}{h}\right) + c_{6,x}\left(\frac{z}{h} - c_{7,x}\right)^2\right]\right\} \quad (21a)$$

$$\xi_z^p = c_{A,z}\exp\left\{-\left[c_{1,z}\left(\frac{x}{h}\right)^2 + c_{2,z}\left(\frac{y}{h}\right) + c_{3,z}\left(\frac{z}{h}\right)^2\right]\right\} + c_{B,z}\exp\left\{-\left[c_{4,z}\left(\frac{x}{h}\right)^2 + c_{5,z}\left(\frac{y}{h}\right) + c_{6,z}\left(\frac{z}{h} - c_{7,z}\right)^2\right]\right\} \quad (21b)$$

where corrective terms ξ_x^p and ξ_z^p consist of two Gaussian functions. Herein, c_A and c_B are the amplitude coefficient, whereas c_1–c_7 are the attenuation factors. Higher $V_{l,t}$ can cause an additional deformation peak in the proximity of the tunnel crown (Franza and Marshall 2015), thereby a second Gaussian function with the center of (x, y, c_7h) is used in the corrective terms. Considering the evolution of deformation along the y direction is asymmetric, thereby the square term is not adopted for y/h.

Herein, the values of coefficients c_i (i = A, B, 1, 2, 3, 4, 5, 6, 7) need to be calibrated for eliminating errors between actual and analytical solution-based results. A metaheuristic optimization algorithm particle swarm optimization (PSO), which has been extensively used in parameters identification (Yagiz and Karahan 2015; Yin et al. 2017), is employed to identify the values of c_i in this study. The introduction of PSO is presented in the Appendix III, and the flowchart of the PSO-based identification of corrective terms is presented in Fig. 6. The position vector of the PSO algorithm is represented by the coefficients c_i. Therefore, the objective of the PSO algorithm is to identify the optimum position vector (c_i) to minimize difference between the ground deformation calculated by analytical solutions and the actual deformation obtained by numerical or experimental modelling. The objective function of PSO is defined as the sum of squared errors (SSE) between actual (y_i) and predicted (μ_i^p) ground deformation:

$$SSE = \sum_{i=1}^{n}\left(\mu_i^p - y_i\right)^2 \quad (22)$$

In reality, the values of c_i are affected by tunnel geometric factors such as cover to diameter ratio, C/D, soil properties such as soil relative density, I_d, and ground deformation status such as ground volume loss,

$V_{l,t}$. Therefore, after the values of c_i are determined and the primary influential factors to coefficients c_i are selected, the correlations between coefficients c_i and these factors deserve to be investigated.

Uniform formulation

From the perspective of published studies, it can be observed that the currently prevailing analytical and semi-analytical solutions for calculating tunneling-induced settlement were developed upon Verruijt and Booker (1996)'s solution, because it can comprehensively account for ground deformation modes. This study first integrates these prevailing analytical, semi-analytical solutions and proposed solutions using a uniform formulation, which can be obtained by:

$$\begin{pmatrix} \mu_x^v \\ \mu_x^\alpha \\ \mu_x^\xi \\ \mu_x^p \end{pmatrix} = \begin{bmatrix} t_x^{11} & t_x^{12} \\ t_x^{21} & t_x^{22} \\ t_x^{31} & t_x^{32} \\ t_x^{41} & t_x^{42} \end{bmatrix} \begin{pmatrix} \varepsilon \\ \delta \end{pmatrix} \tag{23a}$$

$$\begin{pmatrix} \mu_z^v \\ \mu_z^\alpha \\ \mu_z^\xi \\ \mu_z^p \end{pmatrix} = \begin{bmatrix} t_z^{11} & t_z^{12} \\ t_z^{21} & t_z^{22} \\ t_z^{31} & t_z^{32} \\ t_z^{41} & t_z^{42} \end{bmatrix} \begin{pmatrix} \varepsilon \\ \delta \end{pmatrix} \tag{23b}$$

where, μ_x^v, μ_x^α, μ_x^ξ, μ_x^p = horizontal deformation calculated by Verruijt and Booker (1996), González and Sagaseta (2001), Franza and Marshall (2019), and proposed semi-analytical solution in this study, respectively; μ_z^v, μ_z^α, μ_z^ξ, μ_z^p = vertical deformation calculated by the corresponding solutions. ε, δ = normalized uniform convergence and tunnel ovalization deformation. t_x^{ij}, t_z^{ij} (i = 1, 2, 3, 4; j = 1, 2) = termed as deformation coefficients in this study, and they form a deformation matrix. This uniform formulation is able to calculate tunneling-induced settlement such as transverse and longitudinal settlement troughs under various conditions (plain strain or 3-dimension) by changing the values of coefficients in the deformation matrix. Appendix I and II present the deformation matrix for calculating ground deformation in the x-y plane (z = 0) and x-z plane (y = 0), respectively. Therefore, both of tunneling-induced transverse and longitudinal settlement troughs can be predicted using this uniform formulation, and the difference among various solutions can be comprehensively compared.

Case study

Longitudinal settlement trough

Numerical investigation

To validate the applicability of proposed analytical and semi-analytical solutions for predicting tunneling-induced settlement. A 3-dimension numerical model based on finite element method (FEM) software PLAXIS3D is established to generate a series of data. As the 3-dimension FE model in Fig. 7, half section of the tunneling area is modelled since tunnel excavation is a symmetry problem. The tunnel axis runs along the y-direction (from 0 to 100 m). The model laterally extends to a distance of 50 m from the tunnel centerline and vertically extends to a distance of 50 m from the ground surface. The outer and inner diameters of tunnel are 6 and 5.4 m, respectively. The displacement perpendicular to lateral boundaries is restrained while the vertical displacement is allowable. There is no vertical or horizontal displacement along the bottom boundary. The top boundary and the tunnel face boundary are free to move.

Note that this model merely simulates tunneling-induced ground surface deformation in the dry sand. The parameters of the soil constitutive model that is hardening soil (HS) model refers to Zhao et al. (2019), as shown in Table 1. The shield machine and concrete lining are modeled as an isotropic linear elastic material and the continuous concrete lining is simulated. The values of parameters are presented in Table 2. In FE model, the tunnel is excavated at 2 m per step, and the shield machine is 8 m. The face pressure and tail grouting pressure are equal to 1 and 1.2 times horizontal earth pressure, respectively. The tunneling-induced ground volume loss is also simulated by the contraction ratio in PLAXIS3D. It can be seen from Fig. 7 that the contraction ratio along the former 6 m of shield machine increases linearly from zero to the prescribed value, successfully simulating the conicity of shield machine.

The tunneling process consists of following steps: (1) K_0 consolidation, achieving the equilibrium of ground stress; (2) activating the EPB shield, face pressure and grouting pressure; (3) activating excavation step, including freezing face pressure and grouting pressure at current step, excavating 2 m span of soil along the tunnel alignment, installing concrete lining at the rear of the shield machine, moving shield machine, face pressure and grouting pressure to the next position; (4) repeating steps (3) until the completion of tunnel. A total of nine numerical models including C/D of 1, 2, and 3, and $V_{l,t}$ of 1%, 2% and 3% are established for validating proposed analytical and semi-analytical solutions. Tests are labelled according to their C/D ratio and $V_{l,t}$ (i.e. a test with C/D = 1 and $V_{l,t}$ = 1% is labelled CD1V1).

Corrective terms identification

Tunneling-induced longitudinal settlement trough along the tunnel alignment at the ground surface is vitally significant in engineering practice, it is thus investigated in this study. Based on the uniform formulation presented in Appendix I for 3-dimension ground deformation at the ground surface, the deformation matrix for the longitudinal settlement trough along the tunnel alignment at the ground surface can be expressed by:

$$\xi^{p}_{z,x=0,z=0} = c_{A,z}\exp\left[-c_{2,z}\left(\frac{y}{h}\right)^2\right] + c_{B,z}\exp\left[-c_{5,z}\left(\frac{y}{h}\right)^2\right] \tag{24a}$$

$$t^{11}_{z,x=0,z=0} = \frac{R^2(2-2\nu)}{h}\left[1-\frac{y}{\left(y^2+h^2\right)^{1/2}}\right] \tag{24b}$$

$$t_{z,x=0,z=0}^{12}=\frac{R^2}{h}\left[1-\frac{y}{\left(y^2+h^2\right)^{1/2}}\right] \tag{24c}$$

$$t_{z,x=0,z=0}^{21}=R\left(\frac{R}{h}\right)^{2\alpha-1}\left[1-\frac{y}{\left(y^2+h^2\right)^{1/2}}\right] \tag{24d}$$

$$t_{z,x=0,z=0}^{22}=R\left(\frac{R}{h}\right)^{2\alpha-1}\left[1-\frac{y}{\left(y^2+h^2\right)^{1/2}}\right] \tag{24e}$$

$$t_{z,x=0,z=0}^{31}=\xi_{z,x=0,z=0}t_{z,x=0,z=0}^{11} \tag{24f}$$

$$t_{z,x=0,z=0}^{32}=\xi_{z,x=0,z=0}t_{z,x=0,z=0}^{12} \tag{24g}$$

$$t_{z,x=0,z=0}^{41}=\xi_{z,x=0,z=0}^{p}t_{z,x=0,z=0}^{11} \tag{24h}$$

$$t_{z,x=0,z=0}^{42}=\xi_{z,x=0,z=0}^{p}t_{z,x=0,z=0}^{12} \tag{24i}$$

The normalized uniform convergence, ε, and tunnel ovalization deformation, δ are the input parameters for the analytical and semi-analytical solutions. Considering the correlation between $V_{l,t}$ and ε:

$$V_{l,t}=\frac{2\pi R*\varepsilon R}{\pi R^2}=2\varepsilon \tag{25}$$

Hence, the value of ε can be determined based on the value of $V_{l,t}$. Fig. 8 illustrates the deformation contour at a cross-section for C/D = 3, where the tunneling-induced ground deformation has maintained steadily. It can be observed that the maximum deformation occurs at the tunnel crown with the values of approximately 20 mm for $V_{l,t}$ = 1%, 30 mm for $V_{l,t}$ = 2% and 45 mm for the $V_{l,t}$ = 3%, respectively, and the corresponding uniform convergence values εR are 15, 30 and 45 mm, respectively. The consistence between the FE results and the uniform convergence values indicates that the uniform convergence deformation dominates the primary responsibility of tunneling-induced ground deformation and the tunnel ovalization deformation is not discernable. This actually complies with engineering practice, where only the long-term tunnel ovalization deformation is considered (Loganathan and Poulos 1998; Zhao et al. 2019). Therefore, ε

$= 0.5V_{l,t}$ and $\delta = 0$ are employed for the analytical and semi-analytical solutions to compare with numerical results. Note that the ground deformation at the remaining section of tunnel periphery is actually less than that at the tunnel crown, which means that the uniform convergence with $\varepsilon = 0.5V_{l,t}$ slightly overestimates ground deformation. Because soils behavior is modelled by the HS constitutive model instead of a linear elastic constitutive model, the unloading cannot induce the same magnitude of deformation as the deformation at the tunnel crown. Meanwhile the weight of shield body and lining also result in a smaller heave at the invert. This slight error in the uniform convergence is neglected for user-friendly calculation and the resulting prediction error actually can be modified by the corrective terms. Meanwhile, Poisson's ratio and compressibility parameter in the uniform formulation are 0.2 and 1, respectively, as same as the value in the FEM.

It can be seen from Eq. [24a] that three additional parameters need to be identified in the semi-analytical solutions, which are determined by the PSO algorithm as mentioned in the section 3.2. Although the number of iterations is set as 10000 in PSO, the *SSE* value virtually maintains at zero as the number of generation reaches 1000 iteration, as shown in Fig. 9. It is interesting to note that the convergence rate decreases with the increase in $V_{l,t}$ for the same C/D ratio. It reflects the error between numerical and analytical results increase with the increase in the $V_{l,t}$, and the details will be revealed in the next section.

The optimum coefficients c_i are obtained when the *SSE* values reach the minimum values, and they will be used to modify corrective terms ξ_x^p and ξ_z^p. As mentioned in the section 3.2, the values of c_i are related to numerous factors. C/D ratio and $V_{l,t}$ are the only variables in the numerical models, an obvious linear relationship between c_i and $V_{l,t}$ for various C/D ratio is observed, which can be expressed by:

$$c_i = p_i * V_{l,t} + q_i \tag{26}$$

where p_i and q_i = fitted parameters, and the corresponding values are presented in Table 3. This relationship is important, because it provides a straightforward method to estimate coefficients c_i based on the tunnel geometric and ground deformation factors, and further better predict tunneling-induced settlement. It should be noted that the values of coefficients presented in Table 3 based on numerical results, thereby they have limited application scopes. However, the method proposed in this study is recommended to investigate the relationships between empirical coefficients and influential factors in various problems, thereby assigns physical meaning to these empirical coefficients and extends their application scope.

Validation results

Fig. 10 presents the results of predicted longitudinal settlement troughs by the uniform formulation including analytical and semi-analytical solutions, compared with results of nine FE models. Franza and Marshall (2019)'s semi-analytical solution μ_z^{ξ} cannot be used to calculate~~d~~ longitudinal settlement trough. Therefore, Fig. 10 only presents the predicted results using proposed two analytical and one semi-analytical solutions.

The settlement is normalized by the tunnel radius for comparing the settlement characteristics in various cases. The maximum error is generated by the plastic solution, μ_z^{α}, because the compressibility parameter α of 1 cannot account for plastic deformation and the default incompressible medium (v = 0) in this solution further increases the prediction error. As mentioned above, elastic solution μ_z^{v} with the uniform convergence of $\varepsilon = 0.5V_{l,t}$ overestimates ground deformation, thereby the predicted settlement is larger than the FEM results for very shallow tunnel with C/D = 1, and the prediction error increases with the increase in the $V_{l,t}$. Nevertheless, with the increase in the C/D ratio, the tunneling-induced settlement area gradually expands and the magnitude of maximum settlement also increases in the numerical results, but the ground surface settlement calculated by the elastic analytical solutions decreases with the increasing C/D ratio. Therefore, the increasing C/D ratio leads to the increasing error between analytical and numerical results. Note that the increasing settlement for C/D ratio increasing from 1 to 2 is larger than that for C/D ratio increasing from 2 to 3. The large C/D ratio intensifies the contribution of arching effect on the settlement, the ground surface settlement away from the loosened and soil arching zone thus progressively holds at a steady value (Lin et al. 2019). Regarding the semi-analytical solution, μ_z^p, the predicted settlement shows great agreement with the numerical results, which indicates the feasibility and reliability of proposed semi-analytical solution for predicting tunneling-induced longitudinal settlement trough.

Transverse settlement trough

Centrifuge data

Tunneling-induced transverse settlement data from the centrifuge tests of plain-strain tunneling are utilized in this section (Franza and Marshall 2019). The model tunnel comprised a metallic cylinder with enlarged ends which was covered by a latex sleeve and filled with water. The ground volume loss $V_{l,t}$ was controlled by extracting water from the model tunnel using a volume control system. The surface and subsurface soil displacements were measured by an image-based displacement measurement technique geoPIV. Tests included C/D of 1.3, 2.4, 4.4, and 6.3, I_d of 30% (loose), 50% (medium-dense), and 90% (dense), and ground $V_{l,t}$ of 2% and 5%. All tests used a dry silica sand known as Leighton Buzzard Fraction E. These tests were performed in the 10 m diameter geotechnical centrifuge at the University of Cambridge, and more details can refer to Marshall (2009). Tests are labelled according to their C/D ratio, I_d and $V_{l,t}$ (i.e. a test with C/D = 1.3, I_d = 0.3 and $V_{l,t}$ = 2% is labelled CD6.3ID90V2). Four tests results including CD1.3ID30V2, CD1.3ID30V5, CD1.3ID90V2 and CD2.5ID30V2 are selected and used for validating proposed solutions in this study.

Validation results

The plain-strain centrifuge test merely focused on the tunneling-induced transverse settlement trough, and only the ground surface settlement is investigated in this study. Therefore, based on the results in the Appendix II, the coefficients in the deformation matrix can be expressed by:

$$\begin{aligned}\xi^{p}_{z,y=0,z=0} = & c_{A,z}\exp\left[-c_{1,z}\left(\frac{x}{h}\right)^{2}\right] \\ & + c_{B,z}\exp\left\{-\left[c_{4,z}\left(\frac{x}{h}\right)^{2} + c_{6,z}\left(-c_{7,z}\right)^{2}\right]\right\}\end{aligned} \tag{27a}$$

$$t^{11}_{z,y=0,z=0} = 2R^{2}\,\frac{2(1-\nu)h}{x^{2}+h^{2}} \tag{27b}$$

$$t^{12}_{z,y=0,z=0} = -2R^{2}h\,\frac{x^{2}-h^{2}}{\left(x^{2}+h^{2}\right)^{2}} \tag{27c}$$

$$t^{21}_{z,y=0,z=0} = 2R\left(\frac{R}{h}\right)^{2\alpha-1}\frac{1}{\left(x^{2}+h^{2}\right)^{\alpha}h^{-2\alpha}} \tag{27d}$$

$$t^{22}_{z,y=0,z=0} = 2R\left(\frac{R}{h}\right)^{2\alpha-1}\left[-\frac{x^{2}-h^{2}}{\left(x^{2}+h^{2}\right)^{1+\alpha}h^{-2\alpha}}\right] \tag{27e}$$

$$t^{31}_{z,y=0,z=0} = \xi_{z,y=0,z=0}\,t^{11}_{z,y=0,z=0} \tag{27f}$$

$$t^{32}_{z,y=0,z=0} = \xi_{z,y=0,z=0}\,t^{12}_{z,y=0,z=0} \tag{27g}$$

$$t^{41}_{z,y=0,z=0} = \xi^{p}_{z,y=0,z=0}\,t^{11}_{z,y=0,z=0} \tag{27h}$$

$$t^{42}_{z,y=0,z=0} = \xi^{p}_{z,y=0,z=0}\,t^{12}_{z,y=0,z=0} \tag{27i}$$

where $\nu = 0.5$; the value of α is related to soil dilatancy, thereby the values for sand with $I_d = 0.3$ and 0.9 are equal to 1 and 1.05, respectively. The process of determining the values of coefficients for the determination of proposed corrective terms ξ^{p}_{x} and ξ^{p}_{z} is similar to the former section, thereby it is not presented for brevity. Table 4 presents the values of these coefficients, which is roughly identical to Franza and Marshall (2019)'s results, thereby indicates the reliability of PSO-based parameters identification.

Franza and Marshall (2015) pointed out the horizontal movements measured at the tunnel springline in the centrifuge tests can be neglected when the value of $V_{l,t}$ ranges from 0 to 5%. The assumed ovalization term δ is thus equal to ε. Fig. 11 presents the results of four tests calculated by the proposed uniform formulation. The settlement is also normalized by the tunnel radius. It can be seen from Figs. 11(a) and (d) that analytical solutions broadly deviate from the measured data in the loose sand with low ground volume loss, but this difference is mitigated in the dense sand or the loose sand with large ground volume loss (see Figs. 11(b) and (c)). Tunneling process can induce large plastic deformation around the tunnel due to the stress relief and tail void, and chimney-like displacement is more prominent for the relatively large and shallow tunnel with low value of C/D ratio (Marshall et al. 2012), thereby elastic analytical solutions obviously underestimate settlement in the vicinity of tunnel crown in the loose sand with low ground volume loss. Nevertheless, in the dense sand and the loose sand with large ground volume loss, the contribution of arching effect to the settlement is more pronounced. Compared with Figs. 11(a) and (b), the settlement calculated by analytical solutions increase linearly with the increase in the $V_{l,t}$, but the increase in the measured settlement is lower than that calculated by analytical solutions, which is attributed to the contribution of arching effect. Similar condition can be also observed in the dense sand in Fig. 11(c), in which the measured settlement lowers in comparison with the loose sand in Fig. 11(a). Therefore, the predicted maximum settlement shows great agreement with measured results in the dense sand or the loose sand with large ground volume loss. It can be observed from Fig. 11 that all predicted settlement trough width using analytical solutions is wider than measured results, because the chimney-like displacement mechanism in the sands is responsible for the decrease of the settlement trough width and it is not considered in the elastic analytical solutions. Fig. 11(c) indicates the increase in the compressibility parameter α can effectively decrease the settlement trough width in accordance with the results presented in Fig. 4(b), because this parameter can take the ground plastic deformation into consideration. The predicted settlement using the proposed semi-analytical solution exists great agreement with measured results. The modification of corrective terms in this study effectively improve the accuracy in predicting ground surface settlement with a simpler formulation, compared with Franza and Marshall (2019)'s semi-analytical solution.

Conclusions

This study proposed novel closed-form analytical and semi-analytical solutions for describing tunneling-induced ground deformation induced by the construction of shallow tunnels in dry soils. A comprehensive literature review regarding the empirical, analytical and semi-analytical methods for calculating transverse and longitudinal settlement troughs induced by shallow tunnels construction was first conducted. Thereafter, an elastic analytical solution and a plastic analytical solution with the integration of tunnel ovalization deformation mode for describing tunneling-induced longitudinal settlement trough of the incompressible medium were proposed. Due to the limitation of analytical solutions, a semi-analytical solution based on two corrective terms ξ_x and ξ_z was further developed for refining the vertical and horizontal ground deformation. A uniform formulation was ultimately proposed with the integration of currently prevailing and proposed analytical and semi-analytical solutions. This uniform formulation was convenient to compare the difference among various analytical and semi-analytical solutions. Therefore, a 3-dimension numerical model was established to compare the performance of various solutions in predicting longitudinal settlement trough, and centrifuge test results from a published research was utilized to compare the performance in predicting transverse settlement trough. Both numerical and centrifuge modelling results revealed the deficiency of analytical solutions in predicting tunneling-induced settlement, especially for the prediction of longitudinal settlement trough, and the proposed semi-analytical solution can accurately predict tunneling-induced transverse and longitudinal settlement troughs.

A metaheuristics optimization algorithm particle swarm optimization (PSO) was employed to identify the coefficients of corrective terms ξ_x and ξ_z used in semi-analytical solutions. It is quite interesting that a linear relationship was obtained between these coefficients and their influential factors, i.e. cover-to-diameter ratio and ground volume loss, which provides a straightforward and effective method to estimate coefficients in practice engineering based on the tunnel geometric, soils properties and ground deformation conditions. This method is genetic and reusable, which means that it is able to investigate the relationships between empirical coefficients and influential factors in various issues, thereby assigns physical meaning to these empirical coefficients and improve their applicability scope.

Appendix I. Matrix for ground deformation in the *x*-*y* plane (*z* = 0)

$$\xi_x = c_{A,x}\exp\left\{-\left[c_{1,x}\left(\frac{x}{h}\right)^2 + c_{2,x}\left(\frac{y}{h}\right)\right]\right\} + c_{B,x}\exp\left\{-\left[c_{4,x}\left(\frac{x}{h}\right)^2 + c_{5,x}\left(\frac{y}{h}\right) + c_{6,x}\left(-c_{7,x}\right)^2\right]\right\} \tag{I. 1a}$$

$$\xi_z = c_{A,z}\exp\left\{-\left[c_{1,z}\left(\frac{x}{h}\right)^2 + c_{2,z}\left(\frac{y}{h}\right)\right]\right\} + c_{B,z}\exp\left\{-\left[c_{4,z}\left(\frac{x}{h}\right)^2 + c_{5,z}\left(\frac{y}{h}\right) + c_{6,z}\left(-c_{7,z}\right)^2\right]\right\} \tag{I. 1b}$$

Matrix for horizontal deformation

$$t^{11}_{x,z=0} = -R^2\,\frac{x\left(2-2\nu\right)}{x^2+h^2}\left[1-\frac{y}{\left(x^2+y^2+h^2\right)^{1/2}}\right] \tag{I. 2a}$$

$$t^{12}_{x,z=0} = R^2\left[\frac{x\left(x^2-kh^2\right)}{\left(x^2+h^2\right)^2} - \frac{2h^2x\left(1-2\nu\right)}{\left(2-2\nu\right)\left(x^2+h^2\right)^2}\right]\left[1-\frac{y}{\left(x^2+y^2+h^2\right)^{1/2}}\right] \tag{I. 2b}$$

$$t^{21}_{x,z=0} = -R\left(\frac{R}{h}\right)^{2\alpha-1}\left[\frac{x}{\left(x^2+h^2\right)^{\alpha}h^{1-2\alpha}}\right]\left[1-\frac{y}{\left(x^2+y^2+h^2\right)^{1/2}}\right] \tag{I. 2c}$$

$$t^{22}_{x,z=0} = R\left(\frac{R}{h}\right)^{2\alpha-1}\frac{x}{\left(x^2+h^2\right)^{\alpha}h^{1-2\alpha}}\left(\frac{x^2-h^2}{x^2+h^2}\right)\left[1-\frac{y}{\left(x^2+y^2+h^2\right)^{1/2}}\right] \tag{I. 2d}$$

$$t_x^{31} = \xi_x t_x^{11} \quad \text{(I. 2e)}$$

$$t_x^{32} = \xi_x t_x^{12} \quad \text{(I. 2f)}$$

$$t_x^{41} = \xi_x^p t_x^{11} \quad \text{(I. 2g)}$$

$$t_x^{42} = \xi_x^p t_x^{12} \quad \text{(I. 2h)}$$

Matrix for vertical deformation

$$t_{z=0}^{11} = \frac{R^2 h\left(2-2\nu\right)}{x^2+h^2}\left[1-\frac{y}{\left(x^2+y^2+h^2\right)^{1/2}}\right] \quad \text{(I. 3a)}$$

$$t_{z=0}^{12} = \frac{-R^2 h\left(x^2-h^2\right)}{\left(x^2+h^2\right)^2}\left[1-\frac{y}{\left(x^2+y^2+h^2\right)^{1/2}}\right] \quad \text{(I. 3b)}$$

$$t_{z=0}^{21} = R\left(\frac{R}{h}\right)^{2\alpha-1}\frac{1}{\left(x^2+h^2\right)^{\alpha} h^{-2\alpha}}\left[1-\frac{y}{\left(x^2+y^2+h^2\right)^{1/2}}\right] \quad \text{(I. 3c)}$$

$$t_{z=0}^{22} = -R\left(\frac{R}{h}\right)^{2\alpha-1}\frac{1}{\left(x^2+h^2\right)^{\alpha} h^{-2\alpha}}\left(\frac{x^2-h^2}{x^2+h^2}\right)\left[1-\frac{y}{\left(x^2+y^2+h^2\right)^{1/2}}\right] \quad \text{(I. 3d)}$$

$$t_z^{31} = \xi_z t_z^{11} \quad \text{(I. 3e)}$$

$$t_z^{32} = \xi_z t_z^{12} \quad \text{(I. 3f)}$$

$$t_z^{41} = \xi_z^p t_z^{11} \quad \text{(I. 3g)}$$

$$t_z^{42} = \xi_z^p t_z^{12} \quad \text{(I. 4h)}$$

Appendix II. Matrix for ground deformation in the *x*-*z* plane (*y* = 0)

$$\xi_x = c_{A,x}\exp\left\{-\left[c_{1,x}\left(\frac{x}{h}\right)^2 + c_{3,x}\left(\frac{z}{h}\right)^2\right]\right\} + c_{B,x}\exp\left\{-\left[c_{4,x}\left(\frac{x}{h}\right)^2 + c_{6,x}\left(\frac{z}{h}-c_{7,x}\right)^2\right]\right\} \quad \text{(II. 1a)}$$

$$\xi_z = c_{A,z}\exp\left\{-\left[c_{1,z}\left(\frac{x}{h}\right)^2 + c_{3,z}\left(\frac{z}{h}\right)^2\right]\right\} + c_{B,z}\exp\left\{-\left[c_{4,z}\left(\frac{x}{h}\right)^2 + c_{6,z}\left(\frac{z}{h}-c_{7,z}\right)^2\right]\right\} \quad \text{(II. 1b)}$$

Matrix for horizontal deformation

$$t_x^{11}=-R^2\left(\frac{x}{r_1^2}+\frac{x}{r_2^2}\right)-2R^2\left[\frac{x(1-2\nu)}{r_2^2}-\frac{2xzz_2}{r_2^4}\right] \quad \text{(II. 2a)}$$

$$t_x^{12}=R^2\left[\frac{x\left(x^2-kz_1^2\right)}{r_1^4}+\frac{x\left(x^2-kz_2^2\right)}{r_2^4}\right]-4R^2h\left[\frac{(1-2\nu)z_2x}{(2-2\nu)r_2^4}+\frac{xz(x^2-3z_2^2)}{(2-2\nu)r_2^6}\right] \quad \text{(II. 2b)}$$

$$t_x^{21}=2R\left(\frac{R}{h}\right)^{2\alpha-1}\left(-\frac{x}{2r_1^{2\alpha}h^{1-2\alpha}}-\frac{x}{2r_2^{2\alpha}h^{1-2\alpha}}+\frac{4xzz_2}{2r_2^{2\alpha+2}h^{1-2\alpha}}\right) \quad \text{(II. 2c)}$$

$$t_x^{22}=2R\left(\frac{R}{h}\right)^{2\alpha-1}\left[\frac{x\left(x^2-z_1^2\right)}{2r_1^{2\alpha+2}h^{1-2\alpha}}+\frac{x\left(x^2-z_2^2\right)}{2r_2^{2\alpha+2}h^{1-2\alpha}}-\frac{4xz\left(x^2-3z_2^2\right)}{2r_2^{2\alpha+4}h^{-2\alpha}}\right] \quad \text{(II. 2d)}$$

$$t_x^{31}=\xi_x t_x^{11} \quad \text{(II. 2e)}$$

$$t_x^{32}=\xi_x t_x^{12} \quad \text{(II. 2f)}$$

$$t_x^{41}=\xi_x^p t_x^{11} \quad \text{(II. 2g)}$$

$$t_x^{42}=\xi_x^p t_x^{12} \quad \text{(II. 2h)}$$

Matrix for vertical deformation

$$t_z^{11}=-R^2\left(\frac{z_1}{r_1^2}+\frac{z_2}{r_2^2}\right)+2R^2\left[\frac{2(1-\nu)z_2}{r_2^2}-\frac{z\left(x^2-z_2^2\right)}{r_2^4}\right] \quad \text{(II. 3a)}$$

$$t_z^{12}=R^2\left[\frac{z_1\left(kx^2-z_1^2\right)}{r_1^4}+\frac{z_2\left(kx^2-z_2^2\right)}{r_2^4}\right]-2R^2h\left[\frac{x^2-z_2^2}{r_2^4}+\frac{2zz_2\left(3x^2-z_2^2\right)}{2(1-\nu)r_2^6}\right] \quad \text{(II. 3b)}$$

$$t_z^{21}=2R\left(\frac{R}{h}\right)^{2\alpha-1}\left[-\frac{z_1}{2r_1^{2\alpha}h^{1-2\alpha}}+\frac{z_2}{2r_2^{2\alpha}h^{1-2\alpha}}-\frac{z\left(x^2-z_2^2\right)}{hr_2^{2+2\alpha}}\right] \quad \text{(II. 3c)}$$

$$t_z^{22}=2R\left(\frac{R}{h}\right)^{2\alpha-1}\left[\frac{z_1\left(x^2-z_1^2\right)}{2r_1^{2\alpha+2}h^{1-2\alpha}}+\frac{z_2\left(x^2-z_2^2\right)}{2r_2^{2\alpha+2}h^{1-2\alpha}}-\frac{x^2-z_2^2}{r_2^{2\alpha+2}h^{-2\alpha}}-2zz_2\frac{3x^2-z_2^2}{r_2^{2\alpha+4}h^{-2\alpha}}\right] \quad \text{(II. 3d)}$$

$$t_z^{31}=\xi_z t_z^{11} \quad \text{(II. 3e)}$$

$$t_z^{32}=\xi_z t_z^{12} \quad \text{(II .3f)}$$

$$t_z^{41}=\xi_z^p t_z^{11} \quad \text{(II. 3g)}$$

$$t_z^{42}=\xi_z^p t_z^{12} \quad \text{(II. 3h)}$$

Appendix III. Brief introduction of particle swarm optimization

Particle swarm optimization (PSO) is a metaheuristic optimization algorithm (Kennedy and Eberhart 1995) developed upon simulating search behaviour and social interaction of animals such as fish school and bird flock. PSO algorithm consists of several populations of particles and each particle is represented by its position vector $\boldsymbol{X}_{\mathrm{i}}^{\mathrm{k}}$, velocity vector $\boldsymbol{V}_{\mathrm{i}}^{\mathrm{k}}$, where k is the current generation and i is the ith particle. The predominant objective of PSO algorithm is to search for the optimum fitness value and the corresponding location. The PSO algorithm starts from defining the objective function, and initializing PSO parameters including the size of population, generations, initial velocity vectors and position vectors. Thereafter the position and velocity of each particle are updated with the guidance of its local best position in the search-space and the global best position until the global best fitness value of all population satisfies the termination criteria. Herein, the velocity and position of each particle are updated using the following equations:

$$\boldsymbol{V}_i^{k+1} = \omega * \boldsymbol{V}_i^k + c_1 * r_1 * \left(\boldsymbol{pBest}_i^k - \boldsymbol{X}_i^k \right) + c_2 * r_2 * \left(gBest^k - \boldsymbol{X}_i^k \right) \tag{III. 1}$$

$$\boldsymbol{X}_i^{k+1} = \boldsymbol{X}_i^k + \boldsymbol{V}_i^{k+1} \tag{III. 2}$$

where ω = inertia weight; c_1 = cognitive acceleration coefficient; c_2 = social acceleration coefficient; r_1, r_2 = random numbers within the range [0, 1] complying with uniform distribution; $\boldsymbol{pBest}_{\mathrm{i}}$ = the local best location of the ith particle; $gBest$ = the global best location among all particles.

Data Availability Statement

All data used during the study are available from the corresponding author by request.

Acknowledges

The present work was carried out with the support of National Natural Science Foundation of China (No.

51878267, No. 51938005)

References

Bobet, A. (2001). "Analytical solutions for shallow tunnels in saturated ground." *J Eng Mech-ASCE*, 127(12), 1258-1266.

Celestino, T. B., Gomes, R. A. M. P., and Bortolucci, A. A. (2000). "Errors in ground distortions due to settlement trough adjustment." *Tunnell. Undergr. Space Technol.*, 15(1), 97–100.

Chakeri, H., Unver, B., and Ozcelik, Y. (2014). "A novel relationship for predicting the point of inflexion value in the surface settlement curve." *Tunnell. Undergr. Space Technol.*, 43, 266-275.

Chen, R. P., Lin, X. T., Kang, X., Zhong, Z. Q., Liu, Y., Zhang, P., and Wu, H. N. (2018). "Deformation and stress characteristics of existing twin tunnels induced by close-distance EPBS under-crossing." *Tunnell. Undergr. Space Technol.*, 82, 468-481.

Chen, R. P., Zhang, P., Kang, X., Zhong, Z. Q., Liu, Y., and Wu, H. N. (2019). "Prediction of maximum surface settlement caused by EPB shield tunneling with ANN methods." *Soils Found.*, 59(2), 284–295.

Chen, R. P., Zhang, P., Wu, H. N., Wang, Z. T., and Zhong, Z. Q. (2019). "Prediction of shield tunneling-induced ground settlement using machine learning techniques." *Front. Struct. Civ. Eng.*, 13(6), 1363–1378.

Dindarloo, S. R., and Siami-Irdemoosa, E. (2015). "Maximum surface settlement based classification of shallow tunnels in soft ground." *Tunnell. Undergr. Space Technol.*, 49, 320-327.

Fang, Y., Chen, Z., Tao, L., Cui, J., and Yan, Q. (2019). "Model tests on longitudinal surface settlement caused by shield tunnelling in sandy soil." *Sustain. Cities Soc.*, 47.

Franza, A., and Marshall, A. M. "Analytical investigation of soil deformation patterns above tunnels in sandy soil." *Proc., Proceedings of the XVI ECSMGE Geotechnical Engineering for Infrastructure and Development*, ICE Publishing, 467-472.

Franza, A., and Marshall, A. M. (2019). "Empirical and semi-analytical methods for evaluating tunnelling-induced ground movements in sands." *Tunnell. Undergr. Space Technol.*, 88, 47-62.

Franza, A., and Marshall, A. M. "Semi-analytical prediction of ground movements due to shallow tunnels in sand." *Proc., Proceedings of the XVI ECSMGE Geotechnical Engineering for Infrastructure and Development*, ICE Publishing, 461-466.

Fu, J., Yang, J., Klapperich, H., and Wang, S. (2016). "Analytical prediction of ground movements due to a nonuniform deforming tunnel." *Int. J. Geomech.*, 16(4), 04015089.

González, C., and Sagaseta, C. (2001). "Patterns of soil deformations around tunnels. Application to the extension of Madrid Metro." *Comput. Geotech.*, 28, 445–468.

Hu, X., He, C., Peng, Z., and Yang, W. (2019). "Analysis of ground settlement induced by Earth pressure balance shield tunneling in sandy soils with different water contents." *Sustain. Cities Soc.*, 45, 296-306.

Jacobsz, S. W., Standing, J. R., Mair, R. J., Hagiwara, T., and Sugiyama, T. (2004). "Centrifuge modelling of tunnelling near driven piles." *Soils Found.*, 44(1), 49-56.

Kennedy, J., and Eberhart, R. (1995). "Particle swarm optimization." *IEEE International Conference on Neural Networks*Perth, Australia, 1942-1948.

Lin, X.-T., Chen, R.-P., Wu, H.-N., and Cheng, H.-Z. (2019). "Three-dimensional stress-transfer mechanism and soil arching evolution induced by shield tunneling in sandy ground." *Tunnell. Undergr. Space Technol.*, 93.

Loganathan, N., and Poulos, H. G. (1998). "Analytical prediction for tunneling-induced ground movements in clays." *J. Geotech. Geoenviron. Eng.*, 124(9), 846-856.

Lü, X. L., Su, Z., Huang, M. S., and Zhou, Y. C. (2017). "Strength reduction finite element analysis of a stability of large cross-river shield tunnel face with seepage." *Eur J Environ Civ En*, 1-18.

Mair, R. J., Taylor, R. N., and Bracegirdleb, A. (1993). "Subsurface settlement profiles above tunnels in clays." *Géotechnique*, 43(2), 315–320.

Marshall, A. M. (2009). "Tunnelling in sand and its effect on pipelines and piles." Ph.D., Cambridge University.

Marshall, A. M., Farrell, R., Klar, A., and Mair, R. (2012). "Tunnels in sands: the effect of size, depth and volume loss on greenfield displacements." *Géotechnique*, 62(5), 385-399.

New, B. M., and O'Reilly, M. P. "Tunnelling induced ground movements: predicting their magnitude and effects." *Proc., 4th Int. Conf. On Ground Movements & Structures*, 671–697.

Ng, C. W. W., Boonyarak, T., and Mašín, D. (2013). "Three-dimensional centrifuge and numerical modeling of the interaction between perpendicularly crossing tunnels." *Can. Geotech. J.*, 50(9), 935-946.

Park, K. H. (2004). "Elastic Solution for Tunneling-Induced Ground Movements in Clays." *Int. J. Geomech.*, 4(4), 310-318.

Peck, R. B. "Deep excavations and tunneling in soft ground." *Proc., Proceedings of 7th International Conference on Soil Mechanic and Foundation Engineering* 225–290.

Pinto, F., and Whittle, A. J. (2014). "Ground movements due to shallow tunnels in soft ground. I: analytical solutions." *J. Geotech. Geoenviron.*, 140(4), 04013040.

Sagaseta, C. (1987). "Analysis of undrained soil deformation due to ground loss." *Géotechnique*, 37(3), 301-320.

Sen, B. (1951). "Note on the stresses produced by nuclei of thermo-elastic strain in a semi-infinite elastic solid." *Q. Appl. Math.*, 8(4), 365-369.

Suwansawat, S., and Einstein, H. H. (2007). "Describing settlement troughs over twin tunnels using a superposition technique." *J. Geotech. Geoenviron. Eng.*, 133(4), 445-468.

Verruijt, A. (1997). "A complex variable solution for a deforming circular tunnel in an elastic half-plane." *Int. J. Numer. Anal. Met.*, 21, 77-89.

Verruijt, A., and Booker, J. R. (1996). "Surface settlements due to deformation of a tunnel in an elastic half plane." *Géotechnique*, 48(5), 709-713.

Vorster, T. E., Klar, A., Soga, K., and Mair, R. J. (2005). "Estimating the effects of tunneling on existing pipelines." *J. Geotech. Geoenviron. Eng.*, 131(11), 1399-1410.

Wang, H. N., Wu, L., Jiang, M. J., and Song, F. (2018). "Analytical stress and displacement due to twin tunneling in an elastic semi-infinite ground subjected to surcharge loads." *Int. J. Numer. Anal. Met.*, 42(6), 809-828.

Yagiz, S., and Karahan, H. (2015). "Application of various optimization techniques and comparison of their performances for predicting TBM penetration rate in rock mass." *Int. J Rock Mech. Min.*, 80, 308-315.

Yang, J. S., Liu, B. C., and Wang, M. C. (2004). "Modeling of tunneling-induced ground surface movements using stochastic medium theory." *Tunnell. Undergr. Space Technol.*, 19(2), 113-123.

Yin, Z. Y., Jin, Y. F., S, S. J., and Hicher, P. Y. (2017). "Optimization techniques for identifying soil parameters in geotechnical engineering: comparative study and enhancement." *Int. J. Numer. Anal. Met.*, 42(1), 1-25.

Yuan, W., Fu, H. L., Zhang, J. B., and Huang, Z. (2018). "Analytical prediction for tunneling-induced ground movements with modified deformation pattern." *Int. J. Geomech.*, 18(6), 04018039.

Zhang, P. (2019). "A novel feature selection method based on global sensitivity analysis with application in machine learning-based prediction model." *Appl. Soft Comput.*, 85, 105859.

Zhang, P., Chen, R.-P., Wu, H.-N., and Liu, Y. (2020). "Ground settlement induced by tunneling crossing interface of water-bearing mixed ground: A lesson from Changsha, China." *Tunnell. Undergr. Space Technol.*, 96, 103224.

Zhang, P., Chen, R. P., and Wu, H. N. (2019). "Real-time analysis and regulation of EPB shield steering using Random Forest." *Automat. Constr.*, 106, 102860.

Zhang, Z. G., and Huang, M. S. (2014). "Geotechnical influence on existing subway tunnels induced by multiline tunneling in Shanghai soft soil." *Comput. Geotech.*, 56, 121-132.

Zhao, C., Alimardani Lavasan, A., Barciaga, T., and Schanz, T. (2019). "Mechanized tunneling induced ground movement and its dependency on the tunnel volume loss and soil properties." *Int. J. Numer. Anal. Met.*, 43(4), 781-800.

Zheng, G., Cui, T., Cheng, X., Diao, Y., Zhang, T., Sun, J., and Ge, L. (2017). "Study of the collapse mechanism of shield tunnels due to the failure of segments in sandy ground." *Eng. Fail. Anal.*, 79, 464-490.

Zheng, G., Sun, J., Zhang, T., Fan, Q., Diao, Y., and Zhou, H. (2018). "Eulerian finite element model for stability analysis of circular tunnels in undrained clay." *Eng. Fail. Anal.*, 91, 216-224.

Table

Table 1 Parameters of hardening soil constitutive model

Parameter	Description	Value	Unit
Φ'	Friction angle	25	°
ψ'	Dilatancy angle	0	°
c'	Cohesion	0	kPa
E_{50}^{ref}	Secant stiffness in triaxial test	1E4	kPa
E_{oed}^{ref}	Tangent stiffness for oedometer loading	1E4	kPa
E_{ur}^{ref}	Elastic unloading-reloading stiffness	3E4	kPa
p^{ref}	Reference stress	100	kPa
m	Exponent power	1	
v	Poisson's ratio	0.2	
γ	Soil unit weight	17	kPa
K_0	Coefficient of lateral earth pressure	0.57	

Table 2 Parameters of shield machine and concrete lining

Parameter	Description	Shield machine	Concrete lining
E	Elastic stiffness	23E7	31E6
v	Poisson's ratio	0.2	0.2
γ	Unit weight	49.5	25

Table 3 Values of coefficients in corrective terms for refining longitudinal settlement trough

C/D	$p_{A,z}$	$q_{A,z}$	$p_{B,z}$	$q_{B,z}$	$p_{2,z}$	$q_{2,z}$	$p_{5,z}$	$q_{5,z}$
1	–0.164	1.880	0.267	–1.704	0.007	0.102	0.072	0.352
2	0.408	1. 633	–0.40	–1.735	–0.021	0.078	–0.034	0.414
3	–0.519	4.090	0.371	–2.142	–0.006	0.047	0.033	0.286

Table 4 Values of coefficients in corrective terms for refining transverse settlement trough

C/D	I_d	$p_{A,z}$	$q_{A,z}$	$p_{B,z}$	$q_{B,z}$	$p_{1,z}$	$q_{1,z}$	$p_{4,z}$	$q_{4,z}$	$p_{6,z}$	$q_{6,z}$	$p_{7,z}$	$q_{7,z}$
1.3	0.3	–0.098	1.56	0.12	0	0.36	1	3.1	0	1.3	0	0	0.73
1.3	0.9	–0.085	0.09	0.3	0	0.59	0.87	5.5	0	1.6	0	0	0.73
2.5	0.3	–0.13	2.2	0.1	0	0.12	1.1	3.5	0	0.26	0	0	0.83

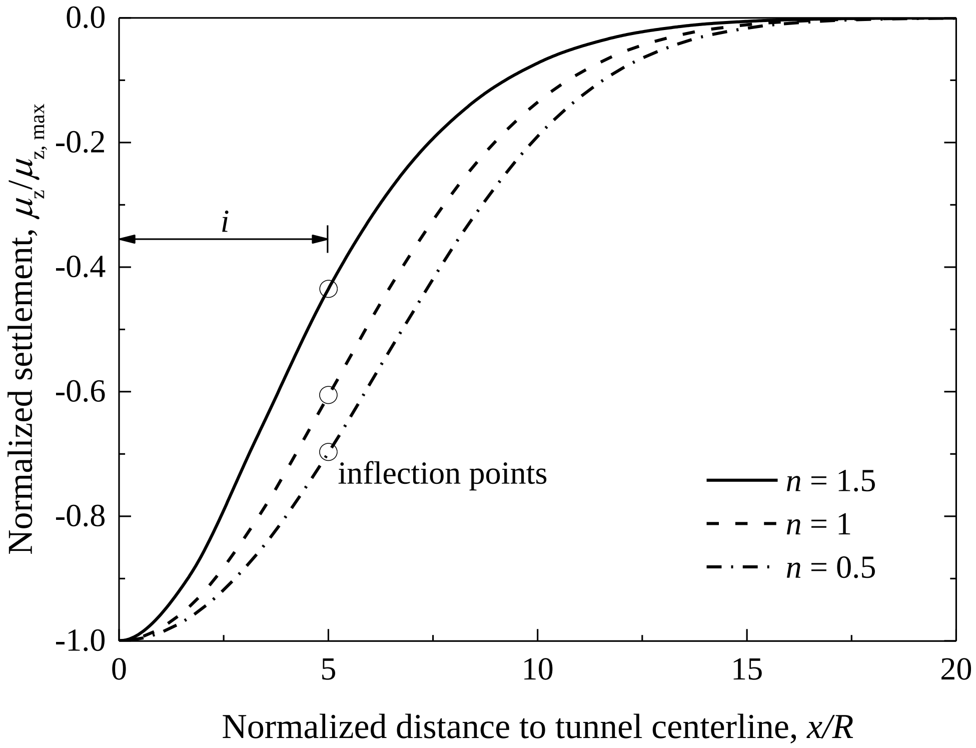
0.0
-0.2
-0.4
-0.6
-0.8
-1.0
0
5
10
15
20
i
inflection points
n = 1.5
n = 1
n = 0.5
Normalized settlement, μz/μz, max
Normalized distance to tunnel centerline, x/R

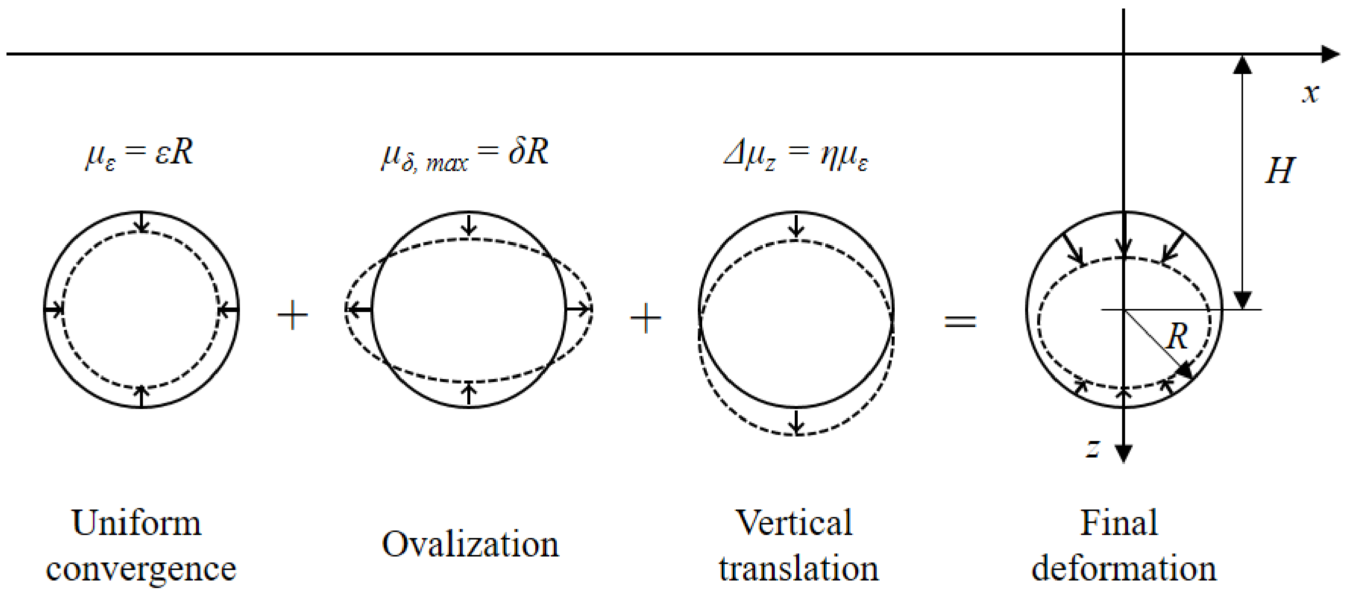

x
H
$\mu_\varepsilon = \varepsilon R$
$\mu_{\delta,\ max} = \delta R$
$\Delta\mu_z = \eta\mu_\varepsilon$
+
+
=
R
z
Uniform convergence
Ovalization
Vertical translation
Final deformation

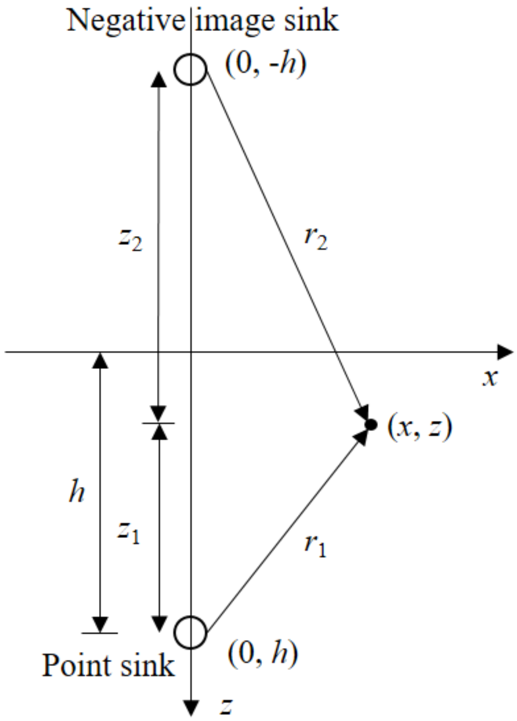
Negative image sink
(0, -h)
z2
r2
x
(x, z)
h
z1
r1
Point sink
(0, h)
z

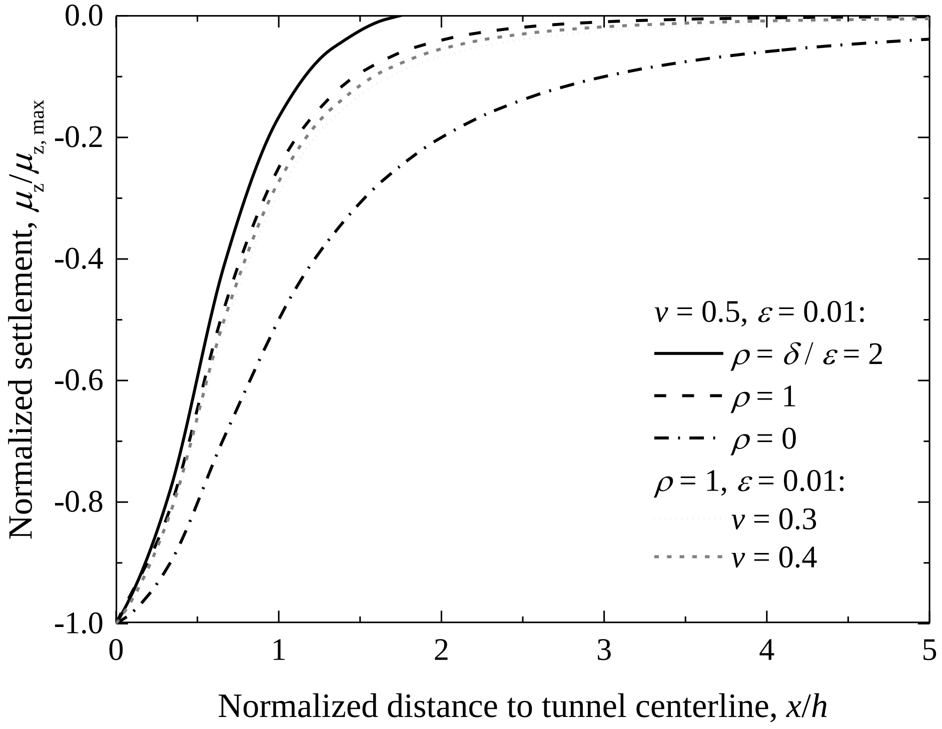

0.0
-0.2
-0.4
-0.6
-0.8
-1.0
0
1
2
3
4
5
Normalized settlement, $\mu_z/\mu_{z,\max}$
Normalized distance to tunnel centerline, x/h
v = 0.5, ε = 0.01:
$\rho = \delta/\varepsilon = 2$
ρ = 1
ρ = 0
ρ = 1, ε = 0.01:
v = 0.3
v = 0.4

(a)

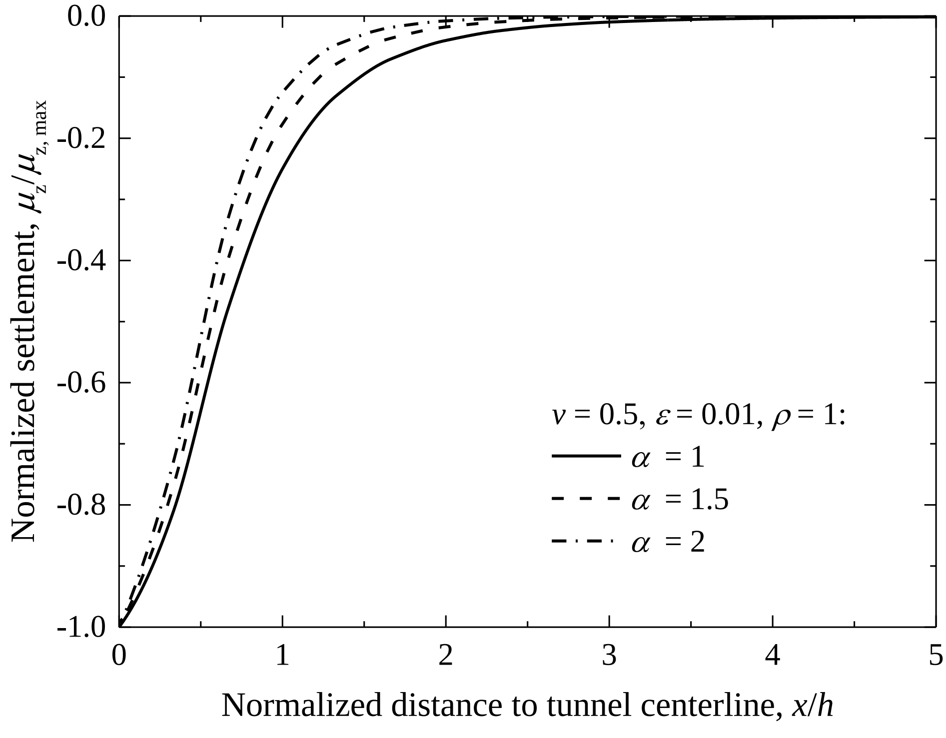

0.0
-0.2
-0.4
-0.6
-0.8
-1.0
0
1
2
3
4
5
Normalized settlement, $\mu_z/\mu_{z,\max}$
Normalized distance to tunnel centerline, x/h
v = 0.5, ε = 0.01, ρ = 1:
α = 1
α = 1.5
α = 2

(b)

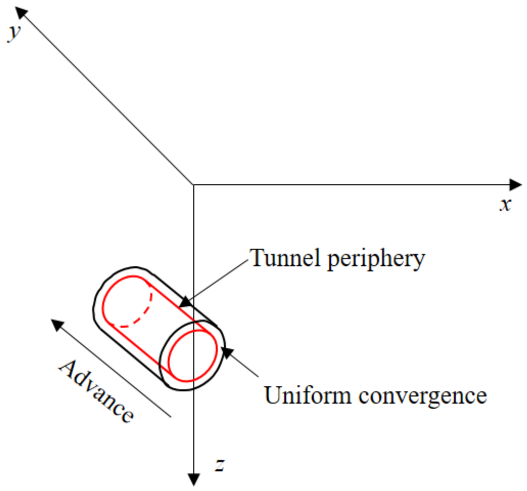
y
x
Tunnel periphery
Advance
Uniform convergence
z

(a)

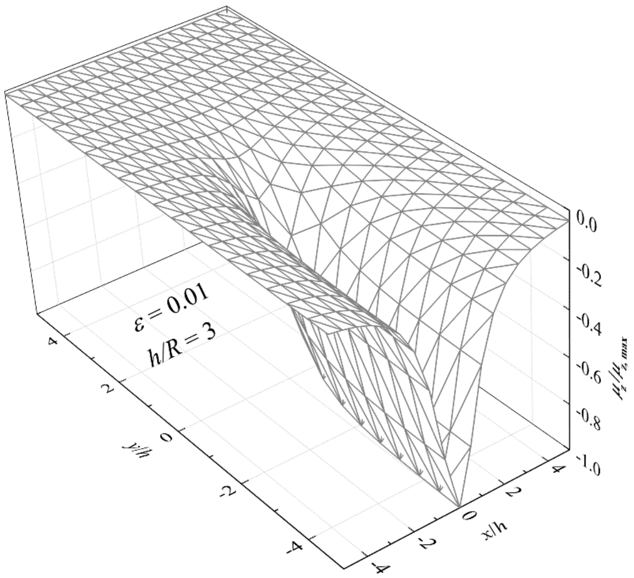
ε = 0.01
h/R = 3
y/h
x/h
0.0
-0.2
-0.4
-0.6
-0.8
-1.0

(b)

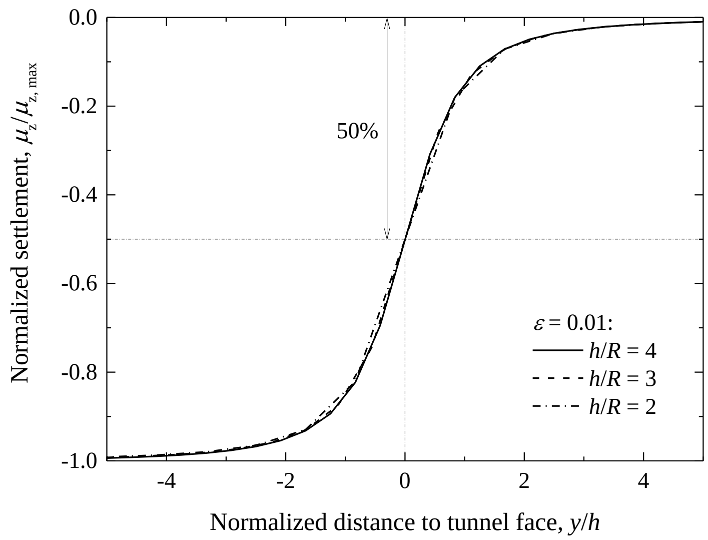
Normalized settlement, μz/μz, max
50%
ε = 0.01:
h/R = 4
h/R = 3
h/R = 2
Normalized distance to tunnel face, y/h

(c)

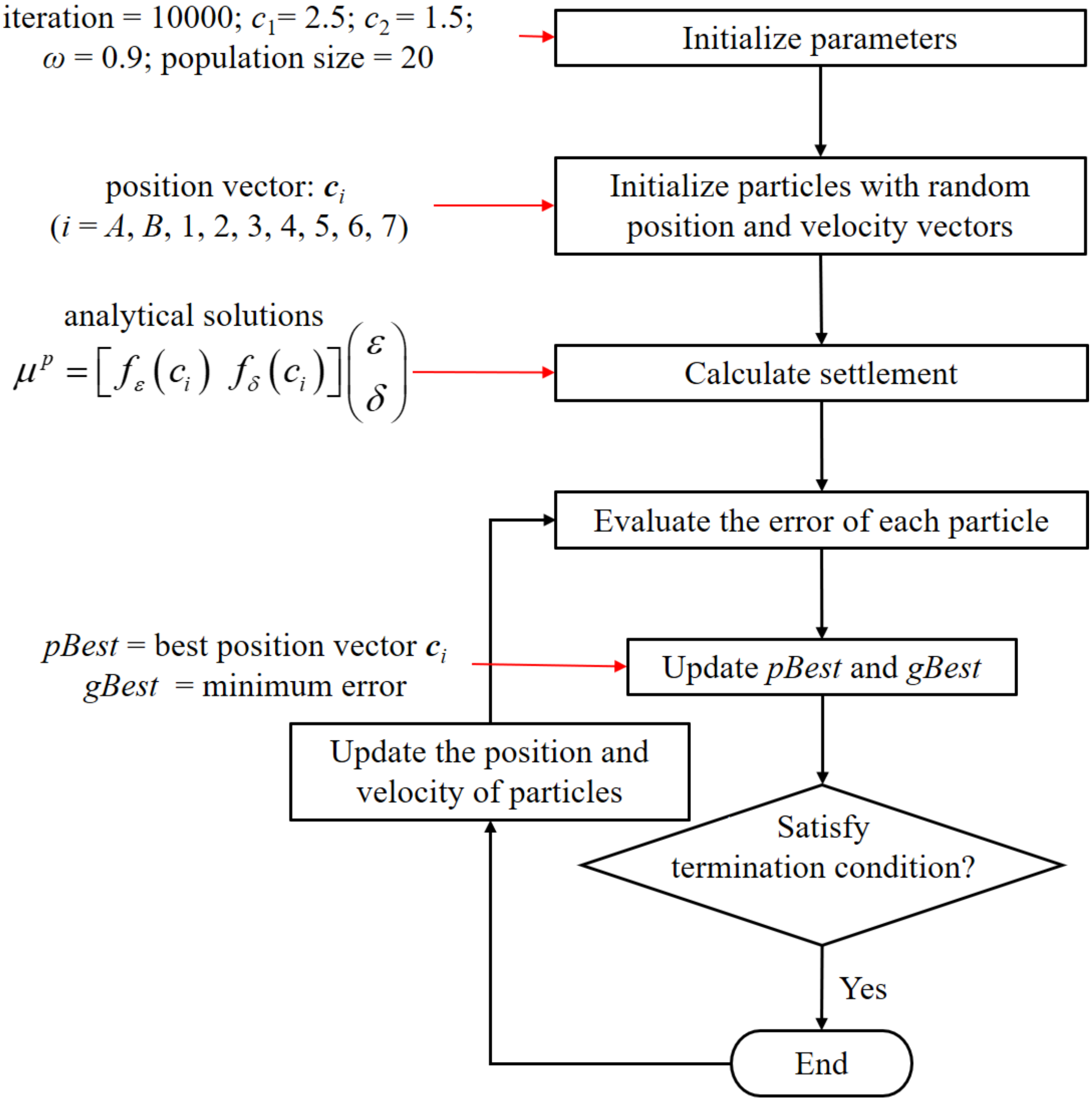
iteration = 10000; c_1= 2.5; c_2 = 1.5;
ω = 0.9; population size = 20
Initialize parameters
position vector: $\boldsymbol{c}_i$
(i = A, B, 1, 2, 3, 4, 5, 6, 7)
Initialize particles with random position and velocity vectors
analytical solutions
$\mu^p = \left[f_\varepsilon(c_i) \;\; f_\delta(c_i) \right] \begin{pmatrix} \varepsilon \\ \delta \end{pmatrix}$
Calculate settlement
Evaluate the error of each particle
$pBest$ = best position vector $\boldsymbol{c}_i$
$gBest$ = minimum error
Update $pBest$ and $gBest$
Update the position and velocity of particles
Satisfy termination condition?
Yes
End

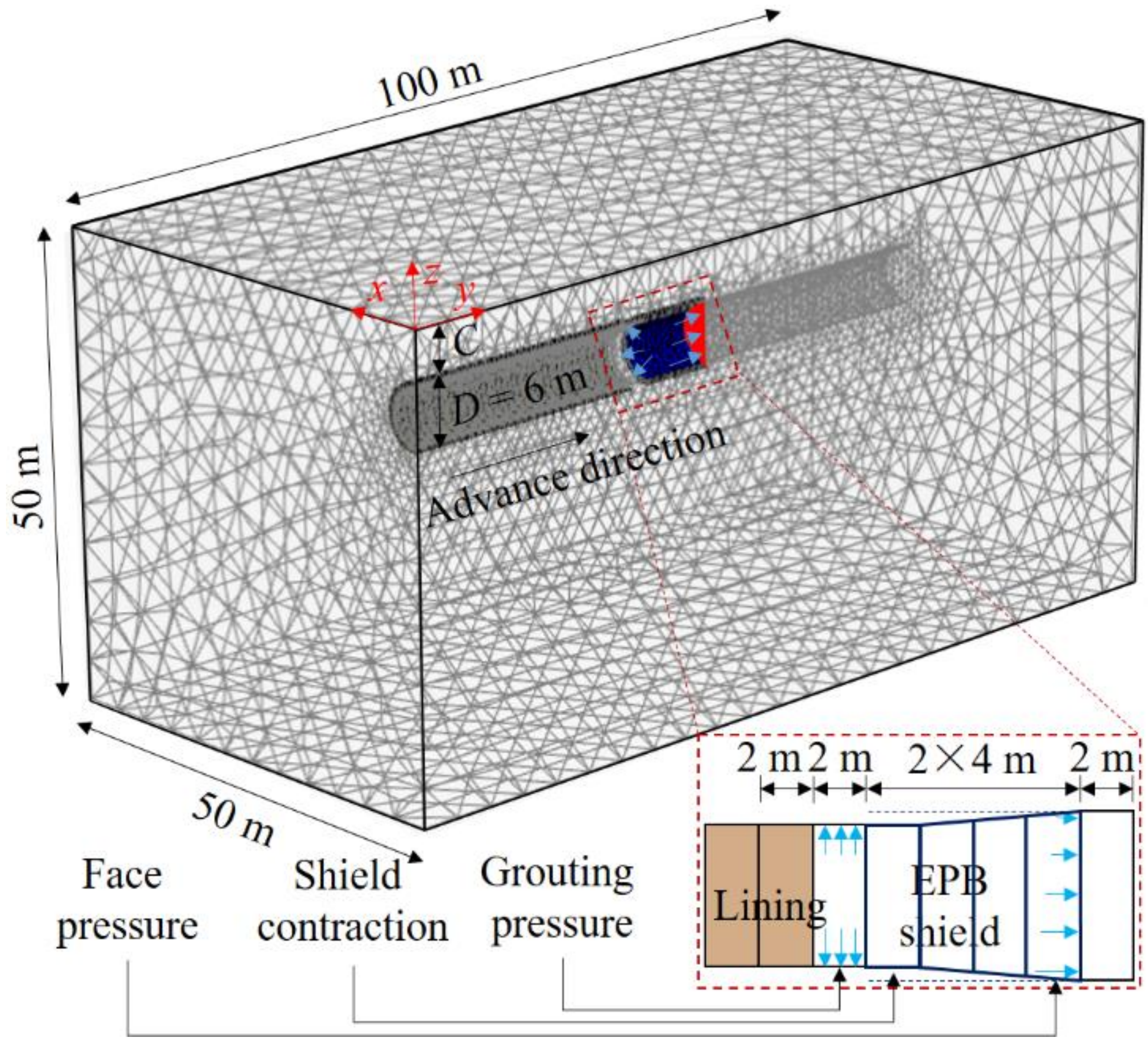
100 m
50 m
50 m
x
z
y
C
D = 6 m
Advance direction
2 m
2 m
2×4 m
2 m
Lining
EPB
shield
Face
pressure
Shield
contraction
Grouting
pressure

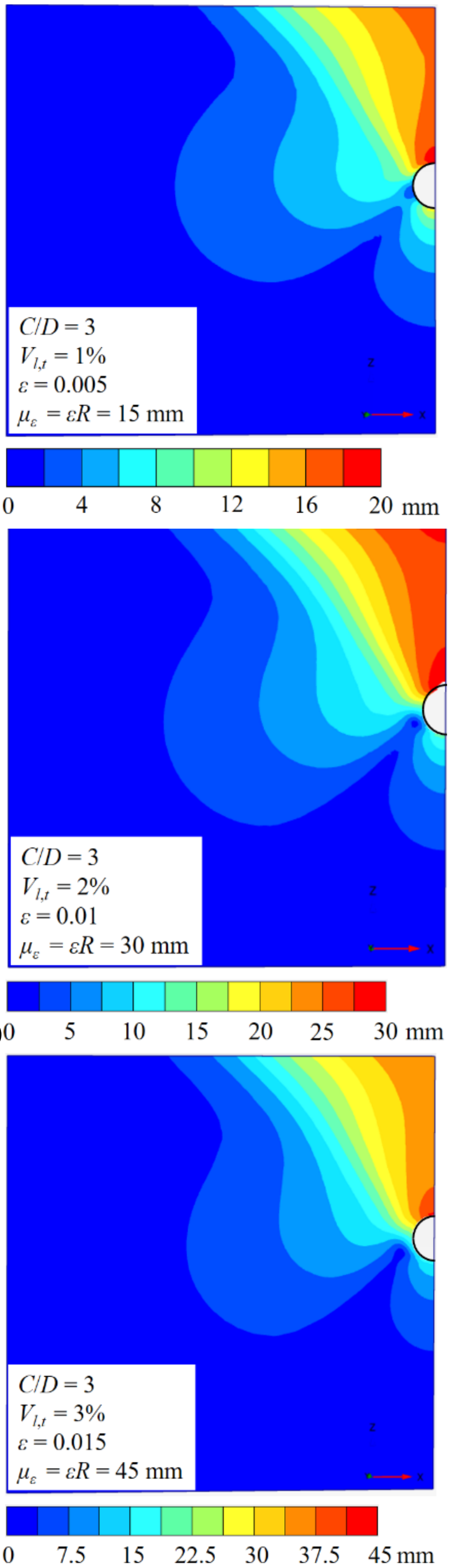

$C/D = 3$
$V_{l,t} = 1\%$
$\varepsilon = 0.005$
$\mu_\varepsilon = \varepsilon R = 15$ mm
0 4 8 12 16 20 mm
$C/D = 3$
$V_{l,t} = 2\%$
$\varepsilon = 0.01$
$\mu_\varepsilon = \varepsilon R = 30$ mm
0 5 10 15 20 25 30 mm
$C/D = 3$
$V_{l,t} = 3\%$
$\varepsilon = 0.015$
$\mu_\varepsilon = \varepsilon R = 45$ mm
0 7.5 15 22.5 30 37.5 45 mm

(a)

(b)

(c)

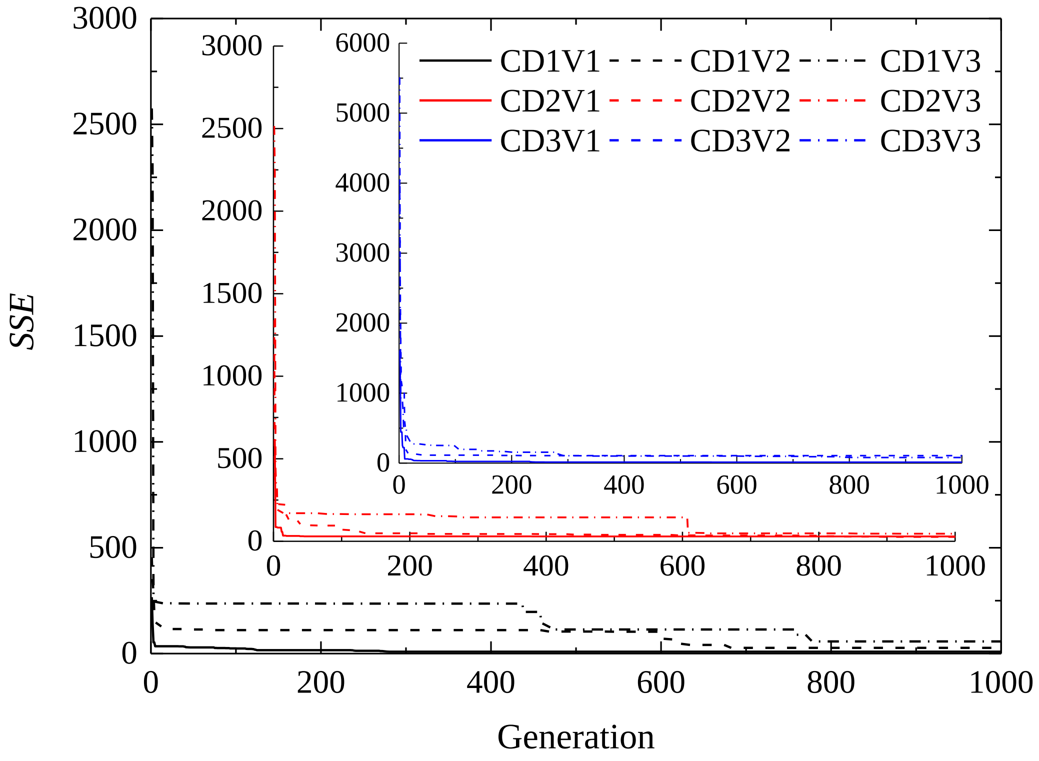

SSE
Generation
CD1V1
CD1V2
CD1V3
CD2V1
CD2V2
CD2V3
CD3V1
CD3V2
CD3V3
0
500
1000
1500
2000
2500
3000
4000
5000
6000
200
400
600
800

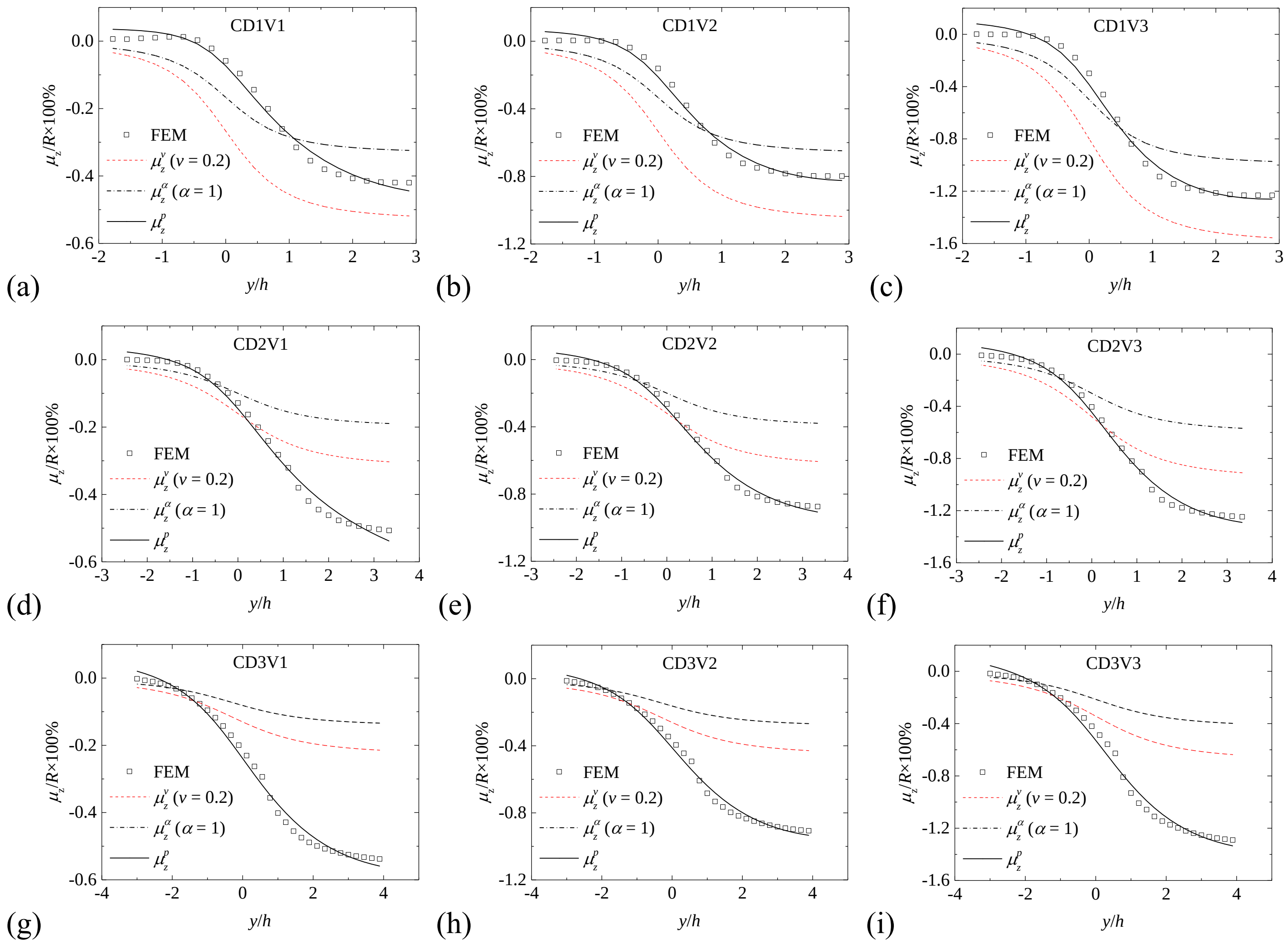

CD1V1
CD1V2
CD1V3
CD2V1
CD2V2
CD2V3
CD3V1
CD3V2
CD3V3
FEM
μ_z^v (v = 0.2)
μ_z^α (α = 1)
μ_z^p
μ_z/R×100%
y/h
(a)
(b)
(c)
(d)
(e)
(f)
(g)
(h)
(i)

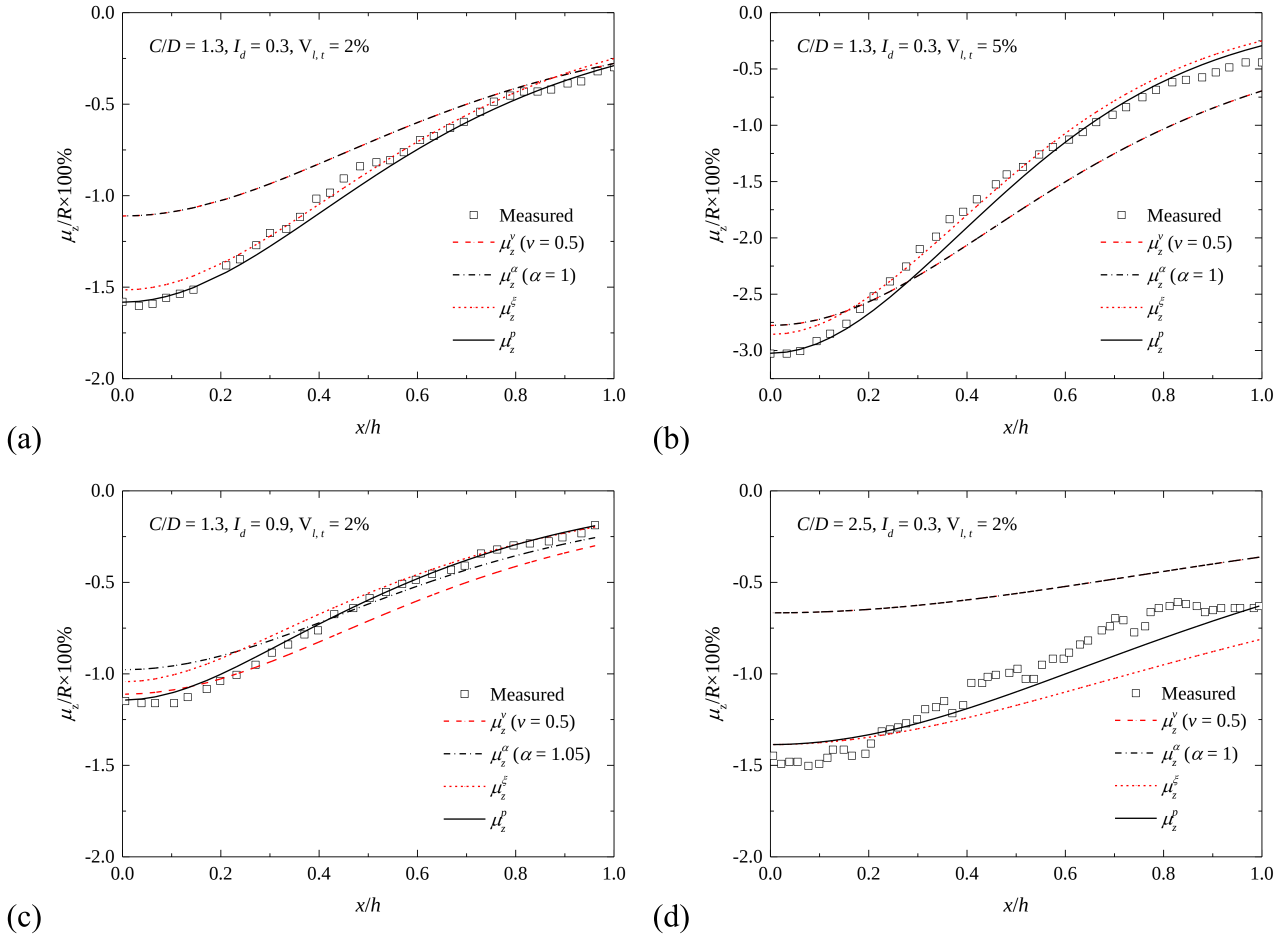

C/D = 1.3, I_d = 0.3, V_l,t = 2%
C/D = 1.3, I_d = 0.3, V_l,t = 5%
C/D = 1.3, I_d = 0.9, V_l,t = 2%
C/D = 2.5, I_d = 0.3, V_l,t = 2%
Measured
μ_z^v (v = 0.5)
μ_z^α (α = 1)
μ_z^α (α = 1.05)
μ_z^ξ
μ_z^p
μ_z/R×100%
x/h
(a)
(b)
(c)
(d)

Figure caption

Fig. 1 Relationship between settlement trough shape predicted by the modified Gaussian curve and *n*

Fig. 2 Deformation mode for shallow tunnel (González and Sagaseta (2001))

Fig. 3 Superposition of point sink and its image sink

Fig. 4 Settlement trough shape predicted by analytical solutions: (a) effects of tunnel ovalization ρ and Poisson's ratio v on the settlement trough shape; (b) effect of compressibility parameter α on the settlement trough shape

Fig. 5 Longitudinal settlement trough: (a) 3-dimensional coordinate; (b) 3-dimensional settlement trough at the ground surface; (c) 2-dimensional longitudinal settlement trough

Fig. 6 Flowchart of PSO-based identification of corrective terms

Fig. 7 Schematic view of 3-dimension finite element model

Fig. 8 Deformation contour at a cross-section for $C/D = 3$

Fig. 9 Evolution of *SSE* values in nine cases

Fig. 10 Comparison between FEM-based longitudinal settlement troughs and predicted settlement troughs using uniform formulation: (a) CD1V1; (b) CD1V2; (c) CD1V3; (d) CD2V1; (e) CD2V2; (f) CD2V3; (g) CD3V1; (h) CD3V2; (i) CD3V3

Fig. 11 Comparison between measured transverse settlement troughs and predicted settlement troughs using uniform formulation: (a) CD1.3ID30V2; (b) CD1.3ID30V5; (c) CD1.3ID90V2; (d) CD2.5ID30V2